รายงานวิจัยฉบับสมบูรณ์

โครงการ การรับแรงร่วมกันระหว่างวัสดุหลักและวัสดุเสริมที่ยึดติดกันแบบไม่สมบูรณ์ในวัสดุเชิงประกอบเสริมด้วยแท่งไพอิโซอิเล็กทริก

โดย รองศาสตราจารย์ ดร.ธีรพงศ์ เสนจันทร์ฒิไชย

เมษายน 2552

สัญญาเลขที่ RMU5080067

รายงานวิจัยฉบับสมบูรณ์

โครงการ การรับแรงร่วมกันระหว่างวัสดุหลักและวัสดุเสริมที่ยึดติดกันแบบไม่สมบูรณ์ในวัสดุเชิงประกอบเสริมด้วยแท่งไพอิโซอิเล็กทริก

โดย รองศาสตราจารย์ ดร.ธีรพงศ์ เสนจันทร์ฒิไชย

ภาควิชาวิศวกรรมโยธา

คณะวิศวกรรมศาสตร์

จุฬาลงกรณ์มหาวิทยาลัย

สนับสนุนโดยสำนักงานกองทุนสนับสนุนการวิจัย

และ สำนักงานคณะกรรมการการอุดมศึกษา

ACKNOWLEDGEMENT

The author would like to acknowledge a research grant from the Thailand Research Fund (TRF) to support the work presented in this report. Grateful acknowledgements are conveyed to Professor R.K.N.D. Rajapakse from the University of British Columbia, Canada for providing helpful comments on this work and Mr. Yasothorn Sapsathiarn for assisting in the development of a computer program and the preparation of this report.

Abstract

Project Code: RMU5080067

Project Title: Matrix-Fiber Interaction in Piezoelectric Fiber-Reinforced Composites with Imperfect Bonding

Investigator: Associate Professor Teerapong Senjuntichai, Ph.D.
Department of Civil Engineering, Faculty of Engineering, Chulalongkorn University

E-mail Address: fcetsj@eng.chula.ac.th

Project Period: 1 year

1-3 piezocomposites are made by embedding piezoelectric fibres/rods in polymeric matrix materials. This class of materials is used in a variety of engineering applications such as ultrasonic transducers, underwater hydrophones, and structural actuators due to their sensing and actuation capabilities. Their performance and reliability are governed by interaction between the piezoelectric phase and surrounding matrix material. It is then important to know the coupled electromechanical behavior of a piezoelectric fiber–matrix system to design composites with enhanced properties. In this research project, two classes of problem are examined. The first problem studies the electromechanical load diffusion from a piezoelectric fiber into a surrounding transversely isotropic elastic matrix due to an axial load and electric charge applied to the fiber. The fiber-matrix interface is assumed to be either mechanically perfect or imperfect, and either electrically open- or short-circuited. The second problem focuses on fracture analysis of the interface cracks in a 1-3 piezoelectric composite by using the displacement discontinuity method (DDM). The study starts with the derivation of analytical solutions for piezoelectric fiber and the transversely isotropic elastic matrix under various loading cases by using Fourier integral transform. These solutions are used to formulate the boundary-value problem of the load diffusion problem and served as a fundamental solution for the DDM in the analysis of interface crack problem. The results for the fiber axial force, electric fields, interfacial stresses and fracture parameters are investigated for representative 1-3 piezocomposites. It is found that the coupled electro-elastic response in piezoelectric fiber-reinforced composites is very complicated and significantly influenced by the properties of the fiber and the matrix, the electrical boundary conditions, and the interface conditions such as imperfect fiber-matrix bonding and the presence of interface cracks. The results from this study provides a fundamental understanding of the coupled electromechanical response from the fiber–matrix interaction in a 1–3 piezocomposite, which are useful for a better design of smart composite materials. In addition, the approach presented in this report can be extended to study more complicated problems such as the investigation of the fiber-to-fiber interaction and the determination of the effective properties of piezoelectric fiber-reinforced composites.

Keywords: Smart materials; piezocomposite; fiber-matrix interaction; imperfect bonding; interface cracks

บทคัดย่อ

รหัสโครงการ: RMU5080067

ชื่อโครงการ: การรับแรงร่วมกันระหว่างวัสดุหลักและวัสดุเสริมที่ยึดติดกันแบบไม่สมบูรณ์ในวัสดุเชิงประกอบเสริมด้วยแท่งไพอิโซอิเล็กทริก

ชื่อนักวิจัย: รองศาสตราจารย์ ดร.ธีรพงศ์ เสนจันทร์ฒิไชย
ภาควิชาวิศวกรรมโยธา คณะวิศวกรรมศาสตร์ จุฬาลงกรณ์มหาวิทยาลัย

E-mail Address: fcetsj@eng.chula.ac.th

ระยะเวลาโครงการ: 1 ปี

วัสดุไพอิโซอิเล็กทริกมีคุณสมบัติในการตอบสนองผลทางกลควบคู่ไปกับผลทางไฟฟ้า ทำให้สามารถนำมาประยุกต์ใช้ในงานด้านการรับส่งสัญญาณหรืออุปกรณ์รับรู้ (Sensor) และอุปกรณ์กระตุ้นเพื่อควบคุมการตอบสนอง (Actuator) ได้หลายประเภท เช่น ไมโครโฟน เครื่องวัดความดันและหน่วยแรง เครื่องวัดความเร่ง เป็นต้น พฤติกรรมของวัสดุเชิงประกอบประเภทนี้มีความซับซ้อนและขึ้นกับปัจจัยหลายอย่าง ได้แก่ ชนิดของวัสดุเสริมและวัสดุหลัก คุณสมบัติของวัสดุแต่ละประเภทและคุณสมบัติของรอยต่อระหว่างวัสดุ ลักษณะและประเภทของแรงกระทำต่อวัสดุเชิงประกอบ เป็นต้น การศึกษาผลของปัจจัยต่าง ๆ ดังกล่าว ต่อพฤติกรรมของวัสดุเชิงประกอบจึงมีความสำคัญอย่างยิ่งในการออกแบบวัสดุเชิงประกอบให้เหมาะสมกับการใช้งาน

โครงการวิจัยนี้ศึกษาอิทธิพลของปัจจัยต่างๆ ต่อพฤติกรรมการถ่ายแรงระหว่างวัสดุในวัสดุเชิงประกอบเสริมด้วยแท่งไพอิโซอิเล็กทริกภายใต้แรงกระทำทางกลหรือโหลดทางไฟฟ้า โดยพิจารณาทั้งกรณีที่วัสดุเสริมและวัสดุหลักของวัสดุเชิงประกอบมีการยึดติดกันแบบสมบูรณ์และแบบไม่สมบูรณ์ รวมทั้งพิจารณาเงื่อนไขขอบเขตทางไฟฟ้าทั้งแบบวงจรปิดและวงจรเปิด งานวิจัยนี้ใช้วิธีการแปลงฟูเรียร์เพื่อวิเคราะห์หาคำตอบทั่วไปสำหรับแต่ละวัสดุของวัสดุเชิงประกอบ จากนั้นนำคำตอบทั่วไปที่ได้มาใช้ในการวิเคราะห์ปัญหาการถ่ายแรงในวัสดุเชิงประกอบ โดยพิจารณาเงื่อนไขตรงรอยต่อระหว่างวัสดุ และศึกษากรณีที่วัสดุเชิงประกอบเกิดรอยแตกที่รอยต่อระหว่างวัสดุหลักและแท่งไพอิโซอิเล็กทริก รอยแตกที่เกิดขึ้นดังกล่าวจะทำให้เกิดหน่วยแรงที่มีความเข้มข้นสูงในวัสดุและสามารถนำไปสู่ความเสียหายของวัสดุเชิงประกอบได้ องค์ความรู้ที่ได้จากโครงการวิจัยนี้จะทำให้สามารถทำนายพฤติกรรมของวัสดุเชิงประกอบได้ดีขึ้น อันจะเกิดประโยชน์ในการพัฒนาการออกแบบสำหรับการประยุกต์ใช้วัสดุเชิงประกอบประเภทนี้ให้เหมาะสมกับงานประเภทต่างๆ ได้ดีขึ้น นอกจากนั้น หลักการที่ใช้ในโครงการนี้ยังสามารถนำไปใช้ศึกษาปัญหาที่มีความซับซ้อนมากขึ้น เช่น การรับแรงร่วมกันระหว่างวัสดุเสริมและการทำนายคุณสมบัติของวัสดุเชิงประกอบประเภทไพอิโซอิเล็กทริก

คำหลัก: วัสดุไพอิโซอิเล็กทริก; วัสดุเชิงประกอบ; การรับแรงร่วมกันระหว่างวัสดุเสริมและวัสดุหลัก; การยึดติดกันแบบไม่สมบูรณ์; รอยแตกที่รอยต่อ

TABLE OF CONTENTS

Page

Page

LIST OF TABLES

Page

LIST OF FIGURES

Page

Page

Page

CHAPTER I

INTRODUCTION

Nowadays, smart materials and smart composites have found increasing applications in the fields of science and engineering such as aerospace structures, intelligent or smart structures, nondestructive testing devices, medical devices, and sensing and actuation applications. Several types of smart materials have already been developed such as piezoelectric materials, shape memory alloys, magenetostrictive or piezomagnetic materials and electro/magneto–rheological fluids, etc. Among others, piezoelectric materials have gained the most attention in practical applications. Piezoelectric materials exhibit electro-mechanical coupling phenomenon such that they produce an electric field when deformed under a mechanical stress (direct piezoelectric effect) and, conversely, undergo deformation when subjected to an electric field (converse piezoelectric effect). For these reasons they are used in a variety of applications including ultrasonic transducers, hydrophones, micropositioning devices, accelerometers, and structural actuators. The most widely used piezoelectric material is lead zirconate titanate (PZT). The properties of some piezoelectric materials are shown in Table 1.1.

Even if the inherent properties of smart materials make them interesting, the bulk single–phase smart materials have several drawbacks that limit their applications. For example, the monolithic piezoceramic material has low fracture strength, high stiffness, high density and difficulty in producing complex shapes. Therefore, composites of smart materials have been developed to overcome such drawbacks and to improve the material properties for extended applications.

The most popular class of smart composites is the piezocomposite, which is the composite containing piezoelectric material with other materials. A common form of piezocomposites is a 1–3 piezocomposite which composes of uniaxially aligned piezoelectric fibers embedded in a polymer matrix (Figure 1.1). This combination of piezoelectric fibers and composite technology aims to overcome

Table 1.1 Material properties of some piezoelectric materials

	$BaTiO_3$	PZT–4	PZT–5H	PZT–6B	PZT–7
c_{11} $(\times 10^{10}\ N/m^2)$	15.0	13.9	12.6	16.8	13.0
c_{33} $(\times 10^{10}\ N/m^2)$	14.6	11.5	11.7	16.3	11.9
c_{12} $(\times 10^{10}\ N/m^2)$	6.6	7.78	7.95	6.0	8.3
c_{13} $(\times 10^{10}\ N/m^2)$	6.6	7.43	8.41	6.0	8.3
c_{44} $(\times 10^{10}\ N/m^2)$	4.4	2.56	2.3	2.71	2.5
e_{31} (C/m^2)	-4.35	-5.2	-6.55	-0.9	-10.3
e_{33} (C/m^2)	17.5	15.1	23.3	7.1	14.7
e_{15} (C/m^2)	11.4	12.7	17.0	4.6	13.5
ε_{11} $(\times 10^{-9}\ F/m)$	9.87	6.45	15.38	3.6	17.1
ε_{33} $(\times 10^{-9}\ F/m)$	11.15	5.62	12.76	3.4	18.6

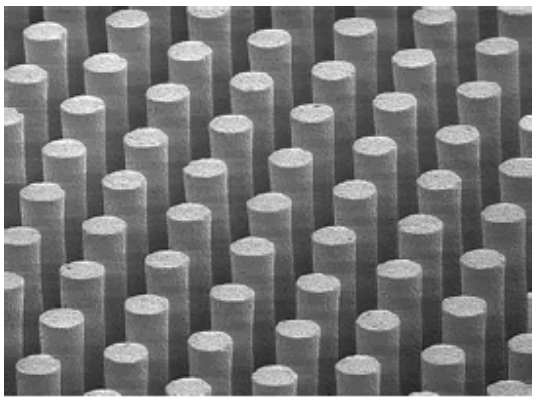

Figure 1.1 A 1–3 piezocomposite.

many poor attributes associated with monolithic piezoceramics. The 1–3 piezocomposite can produce higher electro–mechanical coupling effects, more conformable and less brittle than pure piezoelectric materials. The 1–3 piezocomposite behaves as an anisotropic material. The anisotropic nature of the 1–3 piezocomposite comes from the fact that the response in the fiber direction is dominated by the fiber properties whereas in the transverse direction to the fiber,

the response is dominated by the soft epoxy matrix. The soft epoxy matrix supports the brittle fibers and strengthens the actuator through load sharing. The manufacture of the composites has been improved to achieve high strength and toughness suitable for various applications. Applications for piezocomposite are typically found in the fields of structural actuation for contour control, vibration suppression, and acoustic control, while their sensory nature can be used as a method of structural health monitoring.

The stress analysis of piezoceramics has became increasingly important as their applications are extended to emerging areas such as intelligent structures. The optimum design and reliable operation of intelligent structures require a detailed stress analysis of various composite structural elements containing sensory and actuator layers. Stress concentrations at interfaces, corners and other locations induced by both mechanical and electric loads may lead to the development of critical cracks. In addition, manufacturing defect in piezoceramics is also a contributing factor for brittle failure under external loading. Fundamental understanding of the coupled electro-mechanical interaction between a fiber and a matrix and fracture behavior of the piezocomposite materials is therefore very important to the development of this composite for reliable practical applications.

This research project has two main objectives. The first objective is to obtain the fundamental solutions for the piezoelectric materials and transversely isotropic elastic matrix. These fundamental solutions are very important for the study of several mechanics problems. For example, problems related to fracture, load transfer, delamination, debonding, etc. of piezoelectric composites can be analyzed by developing a series of fundamental solutions corresponding to mechanical loads and an electric charge applied to the piezoelectric fiber and the elastic matrix. Furthermore, the boundary element method can be developed based on these fundamental solutions for analysis of more complicated problems involving piezocomposites. The boundary element method is very effective and efficient in the

stress analysis of complex multi-domain problems such as smart composite elements containing embedded or surface-bonded piezoceramic elements.

The second objective is to study the coupled electromechanical behavior of a piezoelectric fiber–matrix system and the fracture of interfacial cracks in piezocomposites. The problem of a crack or cracks lying at the interface between fiber and matrix is of practical importance in the study of failure of composite materials, because the fracture is commonly observed at such an interface. The analysis of these two fundamental problems can be done by using the general solutions derived in this research project. The results from this study provide the insight understanding the coupling fiber-matrix behavior and fracture mechanics of piezoelectric fiber-reinforced composites.

This research report is organized in the following manner. Chapter 2 presents a survey of related literature on the analysis of piezoelectricity, fiber-matrix interaction and fracture mechanics of piezoelectric materials and composite materials. Chapter 3 summarizes the constitutive equations, the governing equations and presents the general solutions for three dimensional axisymmetric deformation of piezoelectric materials. Chapter 4 presents the application of the general solutions derived in chapter 3 for analysis of electro-mechanical fiber-matrix interaction in piezocomposites. Chapter 5 presents the fundamental solutions for basic interface dislocation problems based on the derived general solutions. These fundamental solutions are used in the displacement discontinuity method for analysis of the interfacial cracks in piezoelectric fiber-reinforced composites. Chapter 6 summarizes the major finding from this research project and the suggestion of the future work related to smart composite materials.

CHAPTER II

SURVEY OF RELATED LITERATURE

Piezoelectric materials have traditionally been used in the development of a variety of electromechanical devices such as pressure transducers and accelerometers. In recent years, these materials have received wide attention due to their immediate relevance to the emerging field of intelligent structures [1, 2]. The concept of an intelligent structure involves an integrated control architecture with highly distributed sensors and actuators. Piezoelectric materials, which produce an electric field when deformed and undergo deformation when subjected to an electric field, are prime candidates for sensors and actuators in an intelligent structure.

Early studies by Mindlin [3], Chen [4], Deeg [5] and others addressed some fundamental problems related to mechanics of piezoelectric materials. The theoretical foundation and electroelastic governing equations of piezoelectric materials were presented by Parton and Kudryavtsev [6]. Thereafter, many researchers provided the theoretical study and analytical solution for plane problem of piezoelectric materials, e.g. Sosa [7], Rajapakse [8], Xu and Rajapakse [9, 10]. Piezoceramic cylinders, which are the common forms of structural elements used in sensor and actuator applications, have also been studied by Rajapakse and Zhou [11] for the case of infinite piezoelectric solid cylinder; and by Rajapakse et al. [12] and Senjuntichai et al. [13] for piezoelectric annular cylinder and solid cylinder respectively.

The low fracture strength, high stiffness, difficulty in producing complex shapes, and high density of the monolithic piezoceramics are all attributes to the development of piezoelectric composites [14, 15]. Performance and reliability of piezocomposites are governed by the interaction between the piezoelectric phase and the surrounding matrix material, which is controlled by several parameters such as the material properties of the two phases, interfacial properties and volume fraction of the piezoelectric phase. The study of the fiber-matrix interaction is then

the key issue for better development of reliable composite materials in advanced engineering applications.

The study of the mechanics of fiber-matrix interaction in traditional composite materials has a rich history. Muki and Sternberg [16] examined the three-dimensional interaction of a single infinitely long cylindrical fiber in an isotropic matrix by studying the diffusion of an axial load from the fiber into the matrix. They gave an exact analytical solution based on the theory of elasticity for a circular fiber and proposed an approximate solution scheme for a fiber with an arbitrary cross section. Thereafter, the load transfer mechanism between fiber and matrix was studied by several researchers such as Pak and Gobert [17], Slaughter and Sanders [18]. In the context of civil engineering, this problem is mathematically identical to the load transfer from a pile into the supporting soil medium [19-21].

The majority of existing works presented in the literature on the mechanics of composite materials is concerned with the classical situation where the displacements and surface tractions are continuous across the fiber–matrix boundary, the so–called perfect bonding condition. It is well known, however, that load transfer between the fiber and the matrix depends significantly on the properties of the so–called interphasial layer (or imperfect interface). The imperfect interface is encountered in the composite materials for various reasons such as thin interphase of adhesion coating, chemical action during manufacturing process, or interfacial damage between the fiber and matrix.

The interphasial layer between fibers and matrix has very complicated microstructure and has different material properties from both the fiber and the matrix. Generally, there are unlikely to have detailed information about the thickness or the material properties of the interphase. Practically, the fiber–matrix interphase moduli are predicted by using an inverse method that requires experimental ultrasonic velocity data together with the results from the theoretical models. Therefore, the theoretical models and the analysis of fiber-reinforced composite with interphasial layer play an important role in both practical

determination of interphase properties using inverse method and the theoretical study of the influence of the fiber–matrix interphase on the responses of the composites. One of the most widely used assumption for describing an imperfect bonding condition is that there are displacement jumps across the interface in which their components are proportional to the corresponding components of the interphasial traction in terms of spring–factor parameters. The spring–factor model for imperfect interface has been initiated in the work by Mal and Bose [22] for the study of the imperfectly bonded elastic spheres. Later, it was employed by Nairn and Liu [23] and Lenci and Menditto [24] among others, for the analysis of elastic fiber–reinforced composites.

Naturally, the fiber–reinforced composites consist of several constituents of different geometry and properties, joined along the interfaces. These factors usually contribute to fracture problems in the composites. The fracture problems of these composites include several crack modes, e.g. fiber cracking, matrix cracking and interfacial cracking. In general, the fiber is strong enough to support the applied load so that cracks are usually formed in the brittle matrix and on the interface between the matrix and fiber. Aveston and his co–authors [25] proposed the ACK model to study the matrix cracking in unidirectional brittle matrix composites. Marshall et al. [26] established qualitatively the relation between the ACK's mechanics of materials model and fracture mechanics as it pertains to brittle matrix composites. McCartney [27] further extended the work of Marshall et al. [26], and established the relation between the matrix–cracking stress and the size of a pre–existing defect. Wijewickrema et al. [28] and Wijewickrema and Keer [29] used this model for the axisymmetric analysis of a fiber embedded in a matrix with annular matrix crack.

The study of interfacial crack has been addressed by a number of investigators. Erdogan and Ozbek [30] used a cylindrical interface dislocation to model a pressurized cylindrical interface crack for an elastic fiber–matrix debonding problem. They carried out the procedure to determine the stress intensity factors

near the crack tip. The pressurized cylindrical crack in transversely isotropic medium was studied later by Kasano et al. [31]. In the above studies, the stress intensity factors and crack opening displacements were evaluated and energy release rates were calculated. Yang and Yuan [32] investigated the interfacial circular crack in cylindrically anisotropic composites subjected to antiplane shear. The pressurized cylindrical crack in a homogeneous isotropic medium has been re–examined lately using a ring dislocation solution [33-35]. These studies yielded numerical solutions for the dislocation distribution, the extended stress field and the stress intensity factors.

The fracture behaviors of piezoelectric ceramics are more complex than that in conventional materials because of the the complicated coupling relationship between mechanical and electric fields [36]. In the study of piezoelectric fractures and failures, available solutions in purely elastic media have been extended to the corresponding problems in piezoelectric materials. Sosa [37] considered a crack in a homogeneous piezoelectric material. Suo et al. [38] considered semi-infinite and finite cracks in a piezoelectric or in an interface between piezoelectric bi-materials. Tian and Rajapakse [39] discussed the axisymmetric problem of an interfacial penny-shaped crack in a piezoelectric bimaterial system. A comprehensive treatment of singularities in multi-material piezoelectric wedges and junctions can be found in Xu and Rajapakse [40].

Most studies on fracture mechanics of piezoelectric solids have been based exclusively on analytical methods. Analytical solutions are mostly restricted to simple geometries and load conditions. Boundary element-based methods for fracture analysis are versatile tools that can be used for the analysis of complex fracture mechanics problems [41]. Pan [42] reported a single-domain BEM formulation for fracture mechanics analysis in cracked 2D piezoelectric solids. Zhao et al. [43] derived the hyper-singular boundary integral–differential equations for planar interface cracks of penny shape in three-dimensional two-phase transversely

isotropic piezoelectric media. The boundary element method was used to solve these equations numerically.

The displacement discontinuity method (DDM) proposed by Crouch and Starfield [44], which is a boundary element method based on a discrete version of the distributed dislocation model of Bilby and Eshelby [45], can be extended to consider fracture mechanics of piezoelectric solids under complex geometry and loading. The DDM has been demonstrated to be successful for two and three dimensional elastostatic [44, 46, 47].

The field intensity factor is an important concept in fracture mechanics. Based on an impermeable crack model, Suo et al. [28] introduced an electric intensity factor for cracks in piezoelectric material in addition to the well known stress intensity factors. For cracks in homogeneous piezoelectric materials, mechanical stresses and the electric displacements show a classical square root singularity at the crack tip. Howerver, cracks at the interface of piezocomposites may contain singularity other than the classcal singularity. Based on the extended Stroh formalism, Suo et al. [28] discussed the singularities of interfacial cracks in bonded anisotropic piezoelectric media. A comprehensive treatment of singularities in multi-material piezoelectric wedges and junctions are also presented by Xu and Rajapakse [40] by extending Lekhnitskii's formalism for elastic anisotropic solids. More recently, Ou [48] and Ou and Chen [49] study the crack-tip singularity of interfacial cracks in transversely isotropic piezoelectric bimaterials and presented the numerical evaluation of the singularity index for composites of commercially available piezoelectric ceramics.

CHAPTER III

BASIC EQUATIONS AND GENERAL SOLUTIONS

In this chapter, the basic equation for piezoelectricity and the governing equations for three–dimensional axisymmetric deformations of a piezoelectric material expressed in terms of displacements and electric potential are presented. The general solutions for axisymmetric deformations of piezoelectric and transversely isotropic elastic materials are then derived by solving the governing equations through the application of Fourier integral transforms. These general solutions will be used to analyze the load transfer problem of fiber–reinforced composite and to derive the fundamental solutions of basic dislocations in the boundary element analysis of interfacial crack in piezoelectric fiber-reinforced composites in the subsequent chapters.

3.1 BASIC EQUATIONS OF AXISYMMETRIC PIEZOELECTRICITY

Consider a composite consisting of an infinite cylindrical piezoelectric fiber of radius "a" embedded in an unbounded transversely isotropic elastic matrix as shown in Figure 3.1. A cylindrical polar coordinate system (r, θ, z) is used with the z–axis is parallel to the axis of the axis of symmetry of fiber and matrix.

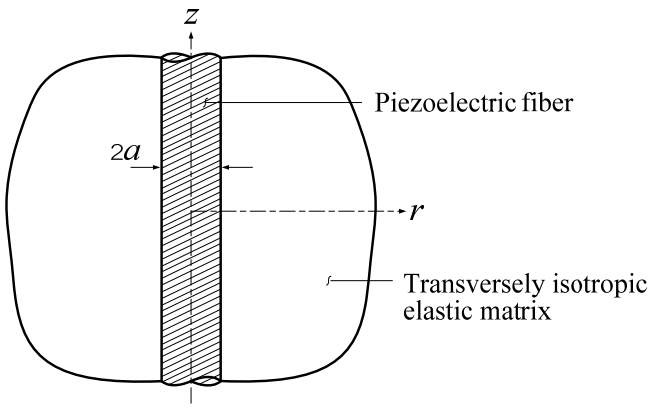

Figure 3.1 Piezoelectric fiber-reinforced composite.

The constitutive equations for a piezoelectric material that are transversely isotropic and poled along the z–axis can be expressed as [6]

$$\sigma_{rr} = c_{11}^f \varepsilon_{rr} + c_{12}^f \varepsilon_{\theta\theta} + c_{13}^f \varepsilon_{zz} - e_{31}^f E_z \tag{3-1a}$$

$$\sigma_{\theta\theta} = c_{12}^f \varepsilon_{rr} + c_{11}^f \varepsilon_{\theta\theta} + c_{13}^f \varepsilon_{zz} - e_{31}^f E_z \tag{3-1b}$$

$$\sigma_{zz} = c_{13}^f \varepsilon_{rr} + c_{13}^f \varepsilon_{\theta\theta} + c_{33}^f \varepsilon_{zz} - e_{33}^f E_z \tag{3-1c}$$

$$\sigma_{rz} = 2c_{44}^f \varepsilon_{rz} - e_{15}^f E_r \tag{3-1d}$$

$$D_z = e_{31}^f \varepsilon_{rr} + e_{31}^f \varepsilon_{\theta\theta} + e_{33}^f \varepsilon_{zz} + \varepsilon_{33}^f E_z \tag{3-1e}$$

$$D_r = 2e_{15}^f \varepsilon_{rz} + \varepsilon_{11}^f E_r \tag{3-1f}$$

where σ_{rr}, $\sigma_{\theta\theta}$, σ_{zz} and σ_{rz} denote the stress components; ε_{rr}, $\varepsilon_{\theta\theta}$, ε_{zz} and ε_{rz} denote the strain components; D_r and D_z denote the electric displacement vectors in the r– and z–directions respectively; E_r and E_z denote the electric fields in the r– and z–directions respectively; c_{11}^f, c_{12}^f, c_{13}^f, c_{33}^f and c_{44}^f denote the elastic constants under zero or constant electric field; e_{31}^f, e_{33}^f and e_{15}^f denote the piezoelectric constants; and ε_{11}^f and ε_{33}^f denote the dielectric constants under zero or constant strain.

It is noted that the constitutive equations for a transversely isotropic matrix material can be obtained from Eqs. (3-1a)–(3-1d) by setting $e_{ij}^f = \varepsilon_{ij}^f \equiv 0$ and replacing c_{ij}^f by c_{ij}^m. The strain–displacement relations are given by

$$\varepsilon_{rr} = \frac{\partial u_r}{\partial r}; \quad \varepsilon_{\theta\theta} = \frac{u_r}{r}; \quad \varepsilon_{zz} = \frac{\partial u_z}{\partial z}; \quad \varepsilon_{zr} = \frac{1}{2}\left(\frac{\partial u_r}{\partial z} + \frac{\partial u_z}{\partial r} \right) \tag{3-2}$$

where u_r and u_z denote the displacements in the r– and z–directions respectively.

The field equations of a piezoelectric material undergoing axisymmetric deformations about the z–axis can be expressed as

$$\frac{\partial \sigma_{rr}}{\partial r} + \frac{\partial \sigma_{rz}}{\partial z} + \frac{\sigma_{rr} - \sigma_{\theta\theta}}{r} + F_r = 0 \tag{3-3a}$$

$$\frac{\partial \sigma_{rz}}{\partial r} + \frac{\partial \sigma_{zz}}{\partial z} + \frac{\sigma_{rz}}{r} + F_z = 0 \tag{3-3b}$$

$$\frac{\partial D_r}{\partial r}+\frac{\partial D_z}{\partial z}+\frac{D_r}{r}+F_E=0 \tag{3-3c}$$

where F_r, F_z and F_E denote the body forces in the $r-$ and $z-$directions and the electric body charge respectively.

The electric field $E_i\,(i=r,z)$ and the electric potential $\phi(r,z)$ are related by

$$E_r=-\frac{\partial \phi}{\partial r};\qquad E_z=-\frac{\partial \phi}{\partial z} \tag{3-4}$$

Substitution of equations (3-1), (3-2) and (3-4) in the field equations (3-3) results in the following governing equations in terms of the displacement u_r and u_z in the $r-$ and $z-$directions and the electric potential $\phi(r,z)$ [11]:

$$c_{11}^f\Big(\frac{\partial^2 u_r}{\partial r^2}+\frac{1}{r}\frac{\partial u_r}{\partial r}-\frac{1}{r^2}u_r\Big)+c_{44}^f\frac{\partial^2 u_r}{\partial z^2}+(c_{13}^f+c_{44}^f)\frac{\partial^2 u_z}{\partial r\partial z}$$
$$+(e_{31}^f+e_{15}^f)\frac{\partial^2 \phi}{\partial r\partial z}+F_r=0 \tag{3-5a}$$

$$c_{44}^f\Big(\frac{\partial^2 u_z}{\partial r^2}+\frac{1}{r}\frac{\partial u_z}{\partial r}\Big)+c_{33}^f\frac{\partial^2 u_z}{\partial z^2}+(c_{13}^f+c_{44}^f)\Big(\frac{\partial^2 u_r}{\partial r\partial z}+\frac{1}{r}\frac{\partial u_r}{\partial z}\Big)$$
$$+e_{15}^f\Big(\frac{\partial^2 \phi}{\partial r^2}+\frac{1}{r}\frac{\partial \phi}{\partial r}\Big)+e_{33}^f\frac{\partial^2 \phi}{\partial z^2}+F_z=0 \tag{3-5b}$$

$$e_{15}^f\Big(\frac{\partial^2 u_z}{\partial r^2}+\frac{1}{r}\frac{\partial u_z}{\partial r}\Big)+e_{33}^f\frac{\partial^2 u_z}{\partial z^2}+(e_{31}^f+e_{15}^f)\Big(\frac{\partial^2 u_r}{\partial r\partial z}+\frac{1}{r}\frac{\partial u_r}{\partial z}\Big)$$
$$-\varepsilon_{11}^f\Big(\frac{\partial^2 \phi}{\partial r^2}+\frac{1}{r}\frac{\partial \phi}{\partial r}\Big)-\varepsilon_{33}^f\frac{\partial^2 \phi}{\partial z^2}-Q=0 \tag{3-5c}$$

3.2 GENERAL SOLUTIONS OF PIEZOELECTRIC MATERIALS

A generalized displacement potential function $\psi(r,z)$ is introduced by relating it to the displacements u_r and u_z, and the electric potential ϕ in the following manner [50]:

$$u_r=\frac{\partial \psi}{\partial r};\qquad u_z=k_1\frac{\partial \psi}{\partial z};\qquad \phi=k_2\frac{\partial \psi}{\partial z} \tag{3-6}$$

where k_1 and k_2 are unknown constants to be determined.

The substitution of equation (3-6) into equations (3-5) results in the following governing equations to determine ψ, k_1 and k_2.

$$\frac{\partial}{\partial r}\left[c_{11}^f\left(\frac{\partial^2\psi}{\partial r^2}+\frac{1}{r}\frac{\partial\psi}{\partial r}\right)+\left\{c_{44}^f+(c_{13}^f+c_{44}^f)k_1+(e_{31}^f+e_{15}^f)k_2\right\}\frac{\partial^2\psi}{\partial z^2}\right] + F_r = 0 \qquad (3\text{-}7a)$$

$$\frac{\partial}{\partial z}\left[\left(c_{13}^f+c_{44}^f+c_{44}^f k_1+e_{15}^f k_2\right)\left(\frac{\partial^2\psi}{\partial r^2}+\frac{1}{r}\frac{\partial\psi}{\partial r}\right)+(c_{33}^f k_1+e_{33}^f k_2)\frac{\partial^2\psi}{\partial z^2}\right] + F_z = 0 \qquad (3\text{-}7b)$$

$$\frac{\partial}{\partial z}\left[\left(e_{31}^f+e_{15}^f+e_{15}^f k_1-\varepsilon_{11}^f k_2\right)\left(\frac{\partial^2\psi}{\partial r^2}+\frac{1}{r}\frac{\partial\psi}{\partial r}\right)+(e_{33}^f k_1-\varepsilon_{33}^f k_2)\frac{\partial^2\psi}{\partial z^2}\right] - Q = 0 \qquad (3\text{-}7c)$$

The solution for the potential function $\psi(r,z)$ composes of the homogeneous solution, denoted by $\psi^h(r,z)$, and the particular solution, denoted by $\psi^p(r,z)$, such that

$$\psi(r,z) = \psi^h(r,z) + \psi^p(r,z) \qquad (3\text{-}8)$$

3.2.1 Homogeneous Solution

The homogeneous solution of the potential function, $\psi^h(r,z)$, is derived from equation (3-7) by setting $F_r = F_z = Q = 0$ and applying Fourier integral transform with respect to z. The Fourier integral transform of a function $f(r,z)$ with respect to z and its inverse are defined by [51]

$$\overline{f}(r,\xi) = \frac{1}{\sqrt{2\pi}}\int_{-\infty}^{\infty} f(r,z)\, e^{i\xi z} dz; \qquad (3\text{-}9a)$$

$$f(r,z) = \frac{1}{\sqrt{2\pi}}\int_{-\infty}^{\infty} \overline{f}(r,\xi)\, e^{-i\xi z} d\xi \qquad (3\text{-}9b)$$

where ξ denotes the Fourier transform parameter.

Applying the Fourier integral transform to equations (3-7) with $F_r = F_z = Q = 0$, the following homogeneous solution can be obtained

$$\overline{\psi}^h(r,\xi) = \sum_{j=1}^{3}\left[I_0(\xi_j r)\, A_j(\xi) + K_0(\xi_j r)\, B_j(\xi)\right] \qquad (3\text{-}10a)$$

where

$$\xi_j = |\xi| \sqrt{\nu_j} \; ; \quad j = 1, 2, 3 \tag{3-10b}$$

and $\bar{\psi}^h$ (j=1,2,3) is the Fourier transform of the homogeneous solution of the potential function; $A_j(\xi)$ and $B_j(\xi)$ (j = 1, 2, 3) are arbitrary functions to be determined from the boundary and continuity conditions; I_n and K_n denote the modified Bessel functions of the first and the second kinds of order n respectively [52]. In addition, the characteristic roots ν_j appearing in equation (3-10) can be determined from the following equation:

$$A\nu^3 + B\nu^2 + C\nu + D = 0 \tag{3-11}$$

where the coefficients A, B, C and D are constants expressed in terms of material properties as

$$A = c_{11}^f \left\{ (e_{15}^f)^2 + c_{44}^f \varepsilon_{11}^f \right\} \tag{3-12a}$$

$$B = c_{13}^f \left\{ 2e_{15}^f (c_{13}^f + 2c_{44}^f) + \varepsilon_{11}^f (c_{13}^f + 2c_{44}^f) \right\} - c_{11}^f (2e_{15}^f e_{33}^f + c_{33}^f \varepsilon_{11}^f + c_{44}^f \varepsilon_{33}^f) \tag{3-12b}$$

$$C = c_{11}^f \left\{ (e_{33}^f)^2 + c_{33}^f \varepsilon_{33}^f) \right\} + c_{13}^f \left\{ 2e_{33}^f (e_{15}^f + e_{31}^f) + \varepsilon_{33}^f (c_{13}^f + 2c_{44}^f) \right\} + c_{33}^f (e_{15}^f + e_{31}^f)^2 + c_{44}^f (2e_{31}^f e_{33}^f - c_{33}^f \varepsilon_{11}^f) \tag{3-12c}$$

$$D = - c_{44}^f \left\{ (e_{33}^f)^2 + c_{33}^f \varepsilon_{33}^f \right\} \tag{3-12d}$$

The three roots of equation (3-11) are denoted by ν_j (j = 1, 2, 3) with ν_1 assumed to be a positive real number, and ν_2 and ν_3 either positive real numbers or a pair of complex conjugates with positive real parts.

Let k_{1j}^h and k_{2j}^h denote the constants k_1 and k_2 of the homogeneous solution corresponding to the root ν_j. It can be shown that

$$k_{1j}^h = \frac{c_{11}^f \nu_j - c_{44}^f - (e_{15}^f + e_{31}^f) k_{2j}^h}{c_{13}^f + c_{44}^f} \tag{3-13a}$$

$$k_{2j}^h = \frac{(c_{11}^f \nu_j - c_{44}^f)(c_{33}^f - c_{44}^f \nu_j) - (c_{13}^f + c_{44}^f)^2 \nu_j}{(e_{15}^f + e_{31}^f)(c_{33}^f - c_{44}^f \nu_j) - (c_{13}^f + c_{44}^f)(e_{33}^f - e_{15}^f \nu_j)} \tag{3-13b}$$

3.2.2 Particular Solution

The particular solutions of the equation (3-7) under a non-zero axial body force and a body charge are derived in this section. This particular solution does not exist in the literature. First, consider the case of a vertical body force $F_z(z)$ in the absence of a radial body force F_r and a body charge Q. To satisfy equation (3-7) for any arbitrary *r*–value, the particular solution ψ^p must be independent of *r*. Consequently, the terms $[(\partial^2\psi^p/\partial r^2)+(1/r)(\partial\psi^p/\partial r)]$ appeared in equation (3-7) must vanish. The constants k_1 and k_2 of the particular solution corresponding to a vertical body force are denoted by k_1^{pz} and k_2^{pz}. These constants can be determined from equations (3-7a) and (3-7c) with $F_r = Q = 0$ as

$$k_1^{pz} = \frac{-c_{44}^f \varepsilon_{33}^f}{(e_{31}^f + e_{15}^f)e_{33}^f + (c_{13}^f + c_{44}^f)\varepsilon_{33}^f}; \quad k_2^{pz} = \frac{e_{33}^f}{\varepsilon_{33}^f} k_1^{pz} \tag{3-14}$$

Applying Fourier transform to equation (3-7b), the following solution for the Fourier transform of the particular solution of the potential function can be obtained.

$$\bar{\psi}^{pz}(\xi) = \frac{i\bar{F}_z(\xi)}{\xi^3(c_{33}^f k_1^{pz} + e_{33}^f k_2^{pz})} \tag{3-15}$$

where $\bar{F}_z(\xi)$ denotes the Fourier transform of the vertical body force.

Let consider the case of an applied electric body charge with $F_r = F_z = 0$. Similar to the case of a vertical body force, the expressions for k_1^{pq} and k_2^{pq} for the case of an electric body charge can be determined from equations (3-7a) and (3-7b) as

$$k_1^{pq} = \frac{c_{44}^f e_{33}^f}{(e_{31}^f + e_{15}^f)c_{33}^f - (c_{13}^f + c_{44}^f)e_{33}^f}; \quad k_2^{pq} = -\frac{c_{33}^f}{e_{33}^f} k_1^{pq} \tag{3-16}$$

The Fourier transform of the particular solution $\bar{\psi}^{pq}$ corresponding to the case of an electric charge $Q(z)$ is obtained from equation (3-7c) as

$$\bar{\psi}^{pq}(\xi) = \frac{-i\bar{Q}(\xi)}{\xi^3(e_{33}^f k_1^{pq} - \varepsilon_{33}^f k_2^{pq})} \tag{3-17}$$

where $\bar{Q}(\xi)$ denotes the Fourier transform of the body charge.

3.2.3 Complete General Solutions

By using the homogeneous and particular solutions presented in the foregoing subsections, the complete general solutions for the Fourier transforms of the electroelastic fields of a solid piezoelectric cylinder can be expressed as

$$\bar{u}_r(r,\xi) = \sum_{j=1}^{3} \xi_j \, I_1(\xi_j r) \, A_j(\xi) \tag{3-18a}$$

$$\bar{u}_z(r,\xi) = -i\xi\left[\sum_{j=1}^{3} k_{1j}^h \, I_0(\xi_j r) A_j(\xi) + k_1^{pz}\bar{\psi}^{pz}(\xi) + k_1^{pq}\bar{\psi}^{pq}(\xi)\right] \tag{3-18b}$$

$$\bar{\phi}(r,\xi) = -i\xi\left[\sum_{j=1}^{3} k_{2j}^h \, I_0(\xi_j r) A_j(\xi) + k_2^{pz}\bar{\psi}^{pz}(\xi) + k_2^{pq}\bar{\psi}^{pq}(\xi)\right] \tag{3-18c}$$

$$\bar{\sigma}_{rr}(r,\xi) = \sum_{j=1}^{3}\left\{|\xi|^2\left[c_{11}^f \nu_j - c_{13}^f k_{1j}^h - e_{31}^f k_{2j}^h\right] I_0(\xi_j r) + (c_{12}^f - c_{11}^f)\xi_j \, r^{-1} I_1(\xi_j r)\right\} A_j(\xi)$$
$$-\xi^2\left[(c_{13}^f k_1^{pz} + e_{31}^f k_2^{pz})\,\bar{\psi}^{pz}(\xi) + (c_{13}^f k_1^{pq} + e_{31}^f k_2^{pq})\,\bar{\psi}^{pq}(\xi)\right] \tag{3-18d}$$

$$\bar{\sigma}_{\theta\theta}(r,\xi) = \sum_{j=1}^{3}\left\{|\xi|^2\left[c_{12}^f \nu_j - c_{13}^f k_{1j}^h - e_{31}^f k_{2j}^h\right] I_0(\xi_j r) + (c_{11}^f - c_{12}^f)\xi_j \, r^{-1} I_1(\xi_j r)\right\} A_j(\xi)$$
$$-\xi^2\left[(c_{13}^f k_1^{pz} + e_{31}^f k_2^{pz})\bar{\psi}^{pz}(\xi) + (c_{13}^f k_1^{pq} + e_{31}^f k_2^{pq})\bar{\psi}^{pq}(\xi)\right] \tag{3-18e}$$

$$\bar{\sigma}_{zz}(r,\xi) = \sum_{j=1}^{3}|\xi|^2\left[c_{13}^f \nu_j - c_{33}^f k_{1j}^h - e_{33}^f k_{2j}^h\right] I_0(\xi_j r) A_j(\xi)$$
$$-\xi^2\left[(c_{33}^f k_1^{pz} + e_{33}^f k_2^{pz})\bar{\psi}^{pz}(\xi) + (c_{33}^f k_1^{pq} + e_{33}^f k_2^{pq})\bar{\psi}^{pq}(\xi)\right] \tag{3-18f}$$

$$\bar{\sigma}_{rz}(r,\xi) = -i\xi\sum_{j=1}^{3}\xi_j\left[c_{44}^f(1+k_{1j}^h) - e_{15}^f k_{2j}^h\right] I_1(\xi_j r) A_j(\xi) \tag{3-18g}$$

$$\bar{D}_r(r,\xi) = -i\xi\sum_{j=1}^{3}\xi_j\left[e_{15}^f(1+k_{1j}^h) - \varepsilon_{11}^f k_{2j}^h\right] I_1(\xi_j r) A_j(\xi) \tag{3-18h}$$

$$\bar{D}_z(r,\xi) = \sum_{j=1}^{3}|\xi|^2\left[e_{31}^f \nu_j - e_{33}^f k_{1j}^h + \varepsilon_{33}^f k_{2j}^h\right] I_0(\xi_j r) A_j(\xi)$$
$$-\xi^2\left[(e_{33}^f k_1^{pz} - \varepsilon_{33}^f k_2^{pz})\bar{\psi}^{pz}(\xi) + (e_{33}^f k_1^{pq} - \varepsilon_{33}^f k_2^{pq})\bar{\psi}^{pq}(\xi)\right] \tag{3-18i}$$

Note that the homogenous general solution given by equation (3-10) corresponds to an infinite annular piezoelectric cylinder. The solution for a solid piezoelectric cylinder of finite radius is obtained from equation (3-10) by setting $B_j = 0$. The remaining three arbitrary functions A_j (j =1, 2, 3) appearing in equation (3-18) can be determined from the three boundary conditions (two mechanical and one electric) associated with the outer surface of a solid piezoelectric cylinder.

3.3 GENERAL SOLUTIONS OF TRANSVERSELY ISOTROPIC ELASTIC MATRIX

Let consider the surrounding matrix in the piezocomposite shown in Figure 3.1. The matrix is transversely isotropic and free from the body forces. The general solution of the transversely isotropic elastic can be derived by following a similar procedure given in Section 3.2 for the piezoelectric case, and setting $e_{ij}^f = \varepsilon_{ij}^f \equiv 0$ and replacing c_{ij}^f by c_{ij}^m. The general solutions for the Fourier transforms of displacements and stresses for a transversely isotropic elastic medium with cylindrical hole are then given by

$$\bar{u}_r(r,\xi) = \sum_{k=1}^{2} \xi_k K_1(\xi_k r)\, C_k(\xi) \tag{3-19a}$$

$$\bar{u}_z(r,\xi) = -i\xi \sum_{k=1}^{2} n_k K_0(\xi_k r) C_k(\xi) \tag{3-19b}$$

$$\bar{\sigma}_{rr}(r,\xi) = \sum_{k=1}^{2} \left\{ |\xi|^2 [c_{11}^m w_k - c_{13}^m n_k] K_0(\xi_k r) - [c_{12}^m - c_{11}^m] \xi_k r^{-1} K_1(\xi_k r) \right\} C_k(\xi) \tag{3-19c}$$

$$\bar{\sigma}_{\theta\theta}(r,\xi) = \sum_{k=1}^{2} \left\{ |\xi|^2 [c_{12}^m w_k - c_{13}^m n_k] K_0(\xi_k r) - [c_{11}^m - c_{12}^m] \xi_k r^{-1} K_1(\xi_k r) \right\} C_k(\xi) \tag{3-19d}$$

$$\bar{\sigma}_{zz}(r,\xi) = \sum_{k=1}^{2} |\xi|^2 [c_{13}^m w_k - c_{33}^m n_k] K_0(\xi_k r) C_k(\xi) \tag{3-19e}$$

$$\bar{\sigma}_{rz}(r,\xi) = i\xi \sum_{k=1}^{2} \xi_k c_{44}^m [1 + n_k] K_1(\xi_k r) C_k(\xi) \tag{3-19f}$$

where c_{ij}^m denotes the elastic constants of the matrix material; $C_k(\xi)$ (k =1, 2) are the arbitrary functions to be determined from the boundary and continuity conditions; and

$$\xi_k = |\xi|\sqrt{w_k}\ ; \qquad n_k = \frac{c_{11}^m w_k - c_{44}^m}{c_{13}^m + c_{44}^m}\ ; \quad k = 1,\ 2 \tag{3-20}$$

In addition, w_k (k =1, 2) are the roots of the following equation

$$c_{11}^m c_{44}^m w_k^2 + \left[\left(c_{13}^m \right)^2 + 2c_{13}^m c_{44}^m - c_{11}^m c_{33}^m \right] w_k + c_{33}^m c_{44}^m = 0 \tag{3-21}$$

CHAPTER IV

ELECTRO-MECHANICAL LOAD TRANSFER IN PIEZOCOMPOSITES

In this chapter, the electro-mechanical interaction between a fiber and a matrix material in a piezocomposite due to an axial load and electric charge applied to the fiber as shown in Figure 4.1 is considered. The fiber-matrix interface is assumed to be mechanically imperfect and is represented by a spring-factor model. The interface is either electrically open- or short-circuited. The general solutions presented in the preceding chapter are used to formulate the load transfer boundary–value problem. Numerical results for the axial force, electric field, displacements and interfacial stresses are presented to demonstrate electromechanical interaction in a fiber–matrix system. Finally, the influence of interface stiffness on the electromechanical load diffusion in piezoelectric fiber-reinforced composite is examined.

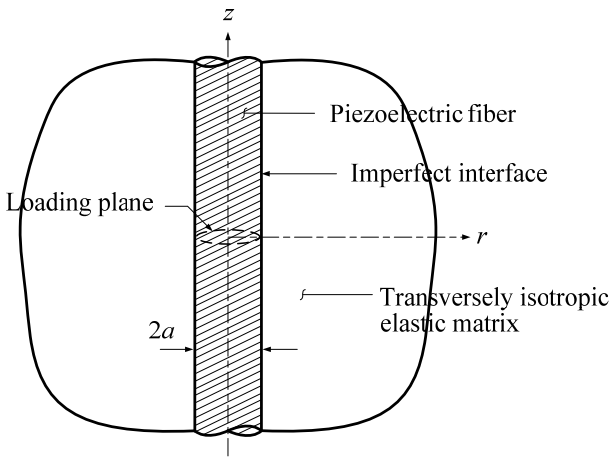

Figure 4.1 Piezoelectric fiber-reinforced composite with imperfect interface.

4.1 PROBLEM FORMULATIONS

The general solutions derived in the Chapter 3 are used in the analysis of the fundamental electro-mechanical fiber-matrix interaction problem shown in Figure 4.1. The fiber–matrix interface is assumed to be either electrically open- or short-circuited, and mechanically imperfect. The general solution of the fiber and matrix are given by equations (3-17) and (3-18) respectively. These equations involve five arbitrary functions, A_1, A_2, A_3, C_1 and C_2, which can be determined from the continuity conditions along the fiber-matrix interface for a specified body force $F_z(z)$ and/or electric charge $Q(z)$. In this study, the fundamental solutions involving an axial force and an electric charge applied uniformly over the fiber cross section at $z=0$ (Figure 4.1) are considered. The total magnitude of the body force and electric charge are P_0 and Q_0 respectively. The corresponding body force functions $F_z(z)$ and $Q(z)$ can be expressed as

$$F_z(z) = -P_0\,\delta(z)/(\pi a^2) \tag{4-1a}$$

$$Q(z) = -Q_0\,\delta(z)/(\pi a^2) \tag{4-1b}$$

The stress continuity conditions and electrically impermeable condition (open-circuit) along the fiber-matrix interface ($r=a$) can be expressed as

$$\sigma_{rr}^{f}(a,z) = \sigma_{rr}^{m}(a,z) \tag{4-2a}$$

$$\sigma_{rz}^{f}(a,z) = \sigma_{rz}^{m}(a,z) \tag{4-2b}$$

$$D_r^{f}(a,z) = 0 \tag{4-2c}$$

in which the superscripts *f* and *m* are used to identify the quantities corresponding to the piezoelectric fiber ($0 \le r \le a$) and the elastic matrix ($a \le r < \infty$) respectively.

Alternately, the electric boundary condition in equation (4-2) can be replaced by $\phi^f(a,z)=0$ that implies short-circuited condition. The two conditions represent the extreme electric boundary conditions at the fiber-matrix interface.

In the present study, the mechanically imperfect fiber-matrix interface is represented by a shear spring-factor model. This model assumes that sufficient cohesion exists on the interface to prevent separation in the radial direction and relates the vertical displacement jump along the interface and the interface shear stress through a spring–factor parameter as follows

$$u_r^f(a,z) = u_r^m(a,z) \tag{4-3a}$$

$$k_s\,[u_z^m(a,z) - u_z^f(a,z)] = \sigma_{rz}^f(a,z) \tag{4-3b}$$

where k_s denotes the spring–factor parameter.

For a perfectly bonded interface, $k_s \to \infty$ and $u_z^f(a,z) = u_z^m(a,z)$. Equations (4-1) – (4-3) can be easily expressed in the Fourier transform domain and the substitution of general solutions given by equations (3-17) and (3-18) in equations (4-2) and (4-3) results in a linear algebraic simultaneous equation system to determine the arbitrary functions A_1, A_2, A_3, C_1 and C_2. Once the arbitrary functions are determined, the full electroelastic field of the system shown in Figure 4.1 can be determined.

Application of the inverse Fourier integral transforms to equation (3-17f) results in the following solution for axial normal stress $\sigma_{zz}^f(r,z)$ in the piezoelectric fiber

$$\sigma_{zz}^f(r,z) = \frac{1}{\sqrt{2\pi}} \int_{-\infty}^{\infty} \Big\{ |\xi|^2 \Big[c_{13}^f v_j - c_{33}^f k_{1j}^h - e_{33}^f k_{2j}^h \Big] I_0(\xi_j r)\, A_j(\xi) - \xi^2 \Big[(c_{33}^f k_1^{pz} + e_{33}^f k_2^{pz})\,\overline{\psi}^{pz}(\xi) + (c_{33}^f k_1^{pq} + e_{33}^f k_2^{pq})\,\overline{\psi}^{pq}(\xi) \Big] \Big\}\, e^{-i\xi z}\, d\xi \tag{4-4}$$

The resultant axial force $P(z)$ in the piezoelectric fiber at a given cross section can be determined from

$$P(z) = 2\pi \int_0^a \sigma_{zz}^f(r,z)\, r\, dr\,; \quad -\infty < z < \infty \tag{4-5}$$

Substitution of the solution of $\sigma_{zz}^f(r,z)$ into equation (4-5) and use of the following identity [52]

$$\int r\, I_0(\xi r)\, dr \;=\; \frac{r\, I_1(\xi r)}{\xi} \tag{4-6}$$

yields

$$P(z) \;=\; \sqrt{2\pi}\; a \int_{-\infty}^{\infty} \Bigg\{ \sum_{j=1}^{3} \frac{|\xi|}{\sqrt{v_j}} (c_{13}^f v_j - c_{33}^f k_{1j}^h - e_{33}^f k_{2j}^h)\; I_1(\xi_j\, a)\, A_j(\xi)$$
$$- \frac{a\xi^2}{2} \Big[(c_{13}^f k_1^{pz} + e_{31}^f k_2^{pz})\; \overline{\psi}^{pz}(\xi) + (c_{13}^f k_1^{pq} + e_{31}^f k_2^{pq})\; \overline{\psi}^{pq}(\xi) \Big] \Bigg\}\; e^{-i\xi z}\, d\xi \tag{4-7}$$

The interfacial shear stress and the electric field along the z-axis are given by

$$\sigma_{rz}(a,z) = \frac{1}{\sqrt{2\pi}} \int_{-\infty}^{\infty} -i\xi \sum_{j=1}^{3} \xi_j \left\{ c_{44}^f (1 + k_{1j}^h) - e_{15}^f k_{2j}^h \right\} I_1(\xi_j\, a)\, A_j(\xi)\, e^{-i\xi z} d\xi \tag{4-8}$$

$$E_z(0,z) = \frac{1}{\sqrt{2\pi}} \int_{-\infty}^{\infty} \xi^2 \left\{ \sum_{j=1}^{3} k_{2j}^h\, A_j(\xi) + k_2^{pz}\, \overline{\psi}^{pz}(\xi) + k_2^{pq}\, \overline{\psi}^{pq}(\xi) \right\} e^{-i\xi z} d\xi \tag{4-9}$$

4.2 NUMERICAL SOLUTIONS

4.2.1 Numerical Scheme

The computation of the electroelastic field corresponding to the problem shown in Figure 4.1 requires the numerical evaluation of infinite integrals involving inverse Fourier transforms. These integrals can be converted to semi–infinite integrals by using the symmetric and anti-symmetric properties of the integrands. In the present study, a globally adaptive numerical quadrature scheme is employed to evaluate the integrals [53]. This scheme subdivides the interval of the integrand and uses a 21–point Gauss–Kronrod rule to estimate the integral over each interval.

The accuracy of the present scheme is first verified by comparing with the existing solutions for an ideal elastic composite system. Elastic composites can be analyzed by using the present scheme by setting the piezoelectric coefficients of the fiber to negligibly small values ($e_{ij} \approx 0$). Figure 4.2 presents a comparison of the numerical solutions for the fibre axial force of a perfectly bonded fiber with those

presented by Muki and Sternberg [16]. The Poisson's ratios of the fiber and matrix are equal to 0.25, and E^f and E^m denote Young's modulus of the fiber and matrix respectively. The solutions presented in Figure 4.2 show an excellent agreement for various values of E^f / E^m confirming the accuracy of the present solution.

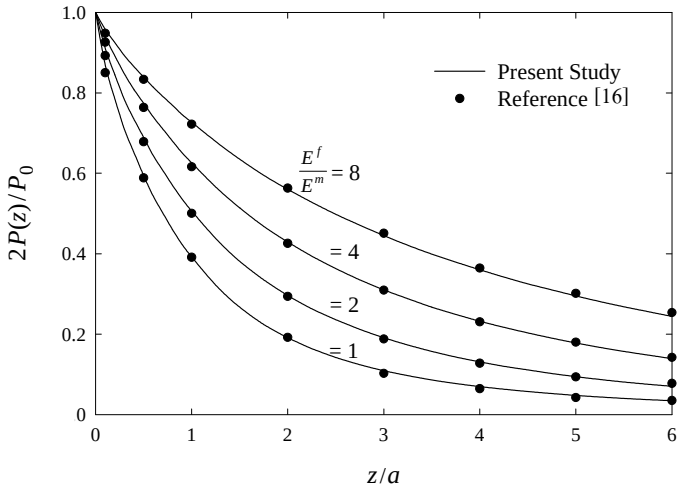

Figure 4.2 Comparison of the fiber axial force for elastic composites.

Further comparisons are presented by considering the case of elastic composites with imperfect fiber-matrix interfaces [24]. The elastic modulus of the fiber, E^f = 68.954 GPa, the matrix Poisson's ratio $\nu = 0.34$ and shear modulus $\mu = 2.59$ GPa. Lenci and Menditto [24] simplified the analysis by modeling the fiber as a one-dimensional bar whereas the present solution allows consideration of the fiber as a 3-D continuum or 1-D bar. A comparison of the fiber axial force, and interfacial shear and radial stresses are presented in Figure 4.3 for various nondimensional interface stiffness values, $E^f/(k_s a)$, in which k_s and a denote the interface stiffness (spring-factor) and radius of the fiber respectively. The results given by Lenci and Menditto [24] and the present scheme agree closely for the fiber axial force and interfacial shear stress as shown in Figures 4.3(a) and (b) respectively. In the case of interfacial radial stress, Figure 4.3(c) shows two solutions obtained from the present scheme: one corresponding to full radial displacement compatibility between the fiber and matrix, and the other with the

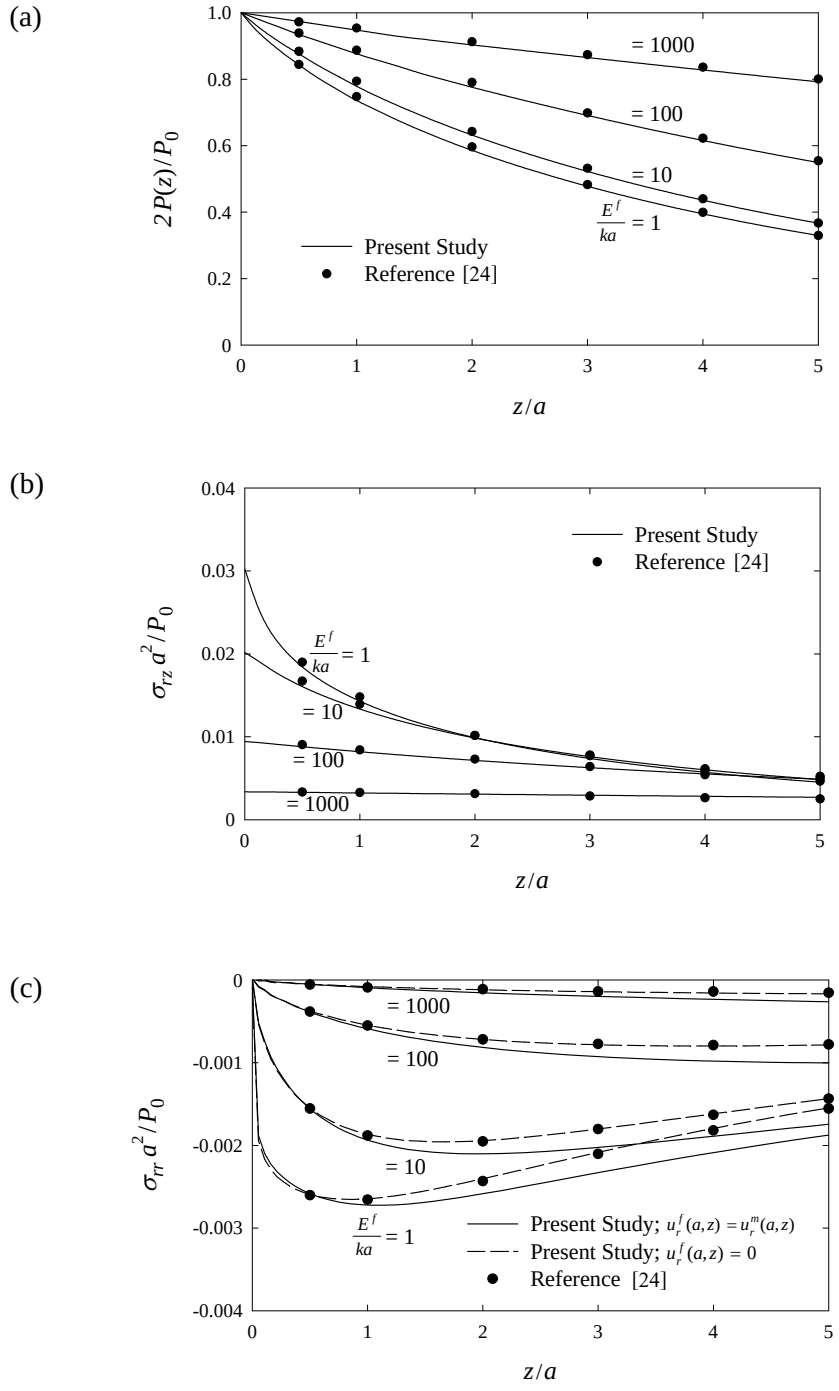

Figure 4.3 Comparison of (a) fiber axial force; (b) interfacial shear stress and (c) interfacial radial stress for an elastic composite with imperfect interface.

constraint that interfacial radial displacement is zero. In the vicinity of the loading plane, the two solutions and the results of [24] agree closely but the differences are noted between the full radial displacement compatibility solution and Ref [24] as z/a

increases. This is due to the fact that the radial deformation is not accounted by the 1-D fiber model of [24]. On the other hand, the present solution for interfacial radial stress with the constraint $u_r^f(a,z)=0$ agrees very closely with the corresponding solution of [24] for all values of *z/a*.

4.2.2 Numerical Results for Force and Charge Diffusion in Piezocomposites

In this section, selected numerical solutions are presented to demonstrate the basic features of the electromechanical load diffusion process in a piezoelectric fiber-reinforced composite. Two elastic polymer matrix materials, identified as matrix A and matrix B, with three different piezoelectric fibers, namely, PZT–6B, PZT–4 and $BaTiO_3$ are used in the numerical study. The properties of piezoelectric materials considered in the numerical study are given in Table 1.1 and the material properties for matrix A and B are given in Table 4.1.

Table 4.1 Material properties of matrix A and matrix B

	c_{11} †	c_{33} †	c_{12} †	c_{13} †	c_{44} †
Matrix A	1.49	4.72	0.66	0.52	0.47
Matrix B	0.2827	0.2827	0.1211	0.1200	0.0808

† $\times 10^{10}\, N/m^2$

The case of piezocomposites with perfect bonding along the fiber-matrix interface is first examined. The corresponding solutions are presented in Figures 4.4–4.9 for fibers with open- and short-circuited conditions along the interface. Note that solutions are presented only for $z \geq 0$ as all quantities are either symmetric or anti-symmetric with respect to the loading plane *z* = 0.

Consider the diffusion of an axial load of magnitude P_0 applied uniformly over the cross section at $z = 0$ of the fiber (Figure 4.1). The variation of nondimensional

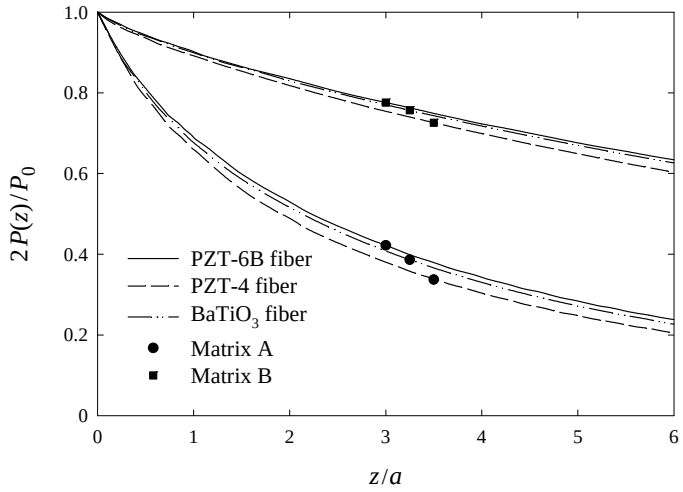

(a)

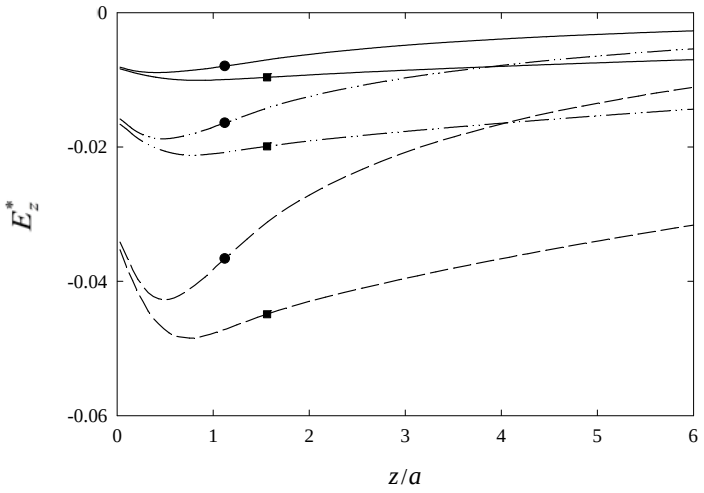

(b)

Figure 4.4 (a) Resultant axial force and (b) vertical electric field along the *z*–axis of piezoelectric fiber (open-circuited) under applied axial load.

resultant axial force along the fiber length is shown in Figure 4.4(a) for the open-circuited case. Naturally the nondimensional axial load has a unit magnitude at $z = 0$ and decreases gradually with z. The decay of axial load in the fiber depends on the type of fiber and matrix material. As the matrix A is stiffer than matrix B (Table

4.1), the axial load is more rapidly transferred to matrix A when compared to matrix B. For example, at a distance six times the fiber–radius from the loading plane, the fiber axial load is approximately 10% and 30% of the applied load for matrix A and matrix B respectively. The dependence of fiber axial load on fiber material properties is quite negligible when compared to its dependence on the matrix material properties.

In the case of piezocomposites, of particular interest to sensor applications are the electric field generated in the fiber due to the applied mechanical loading. Figure 4.4(b) shows the nondimensional vertical electric field, $E_z^* = E_z e_{15}^f a^2 / P_0$, along the axis of the piezoelectric fiber. The peak value of vertical electric field occurs near the loading plane ($z/a < 1$) and thereafter E_z^* gradually decreases with z. The decay of E_z^* along the fiber length is significantly affected by the properties of the fiber and matrix. The PZT-4 fiber has the highest E_z^* followed by the $BaTiO_3$ and PZT–6B fibers, which implies that PZT-4 is more suitable for applications involving sensing. A softer matrix material results in a higher vertical electric field in the fiber as lesser load is transferred to the matrix. In addition, the decay of electric field is relatively slow in the case of a softer matrix allowing better sensing properties.

The variation of nondimensional shear stress, $\sigma_{rz}^* = \sigma_{rz} a^2 / P_0$, and radial stress, $\sigma_{rr}^* = \sigma_{rr} a^2 / P_0$, along the fiber–matrix interface ($r/a = 1$) is shown in Figures 4.5(a) and 4.5(b) respectively. Similar to the case of the fiber axial force, interfacial stresses are mostly influenced by the matrix material when compared to the properties of the fiber. Shear stress along the interface has its maximum value at the loading plane and decreases rapidly in the vertical (fiber) direction. Stiffer matrix materials result in higher interfacial stresses as the load transfer to the matrix is more rapid in this case. Consequently, such composites are more prone to interfacial failure provided that the shear strength at the interface is the same. Radial stress along the fiber-matrix interface is zero at $z = 0$ and increases rapidly with z reaching a peak value near $z/a = 1$ and thereafter decreases rapidly with z.

The peak value of the interface radial stress is less than 10% of the peak interface shear stress. Therefore, interfacial strength is mostly governed by the cohesion at the interface instead of Coulomb friction in the present model.

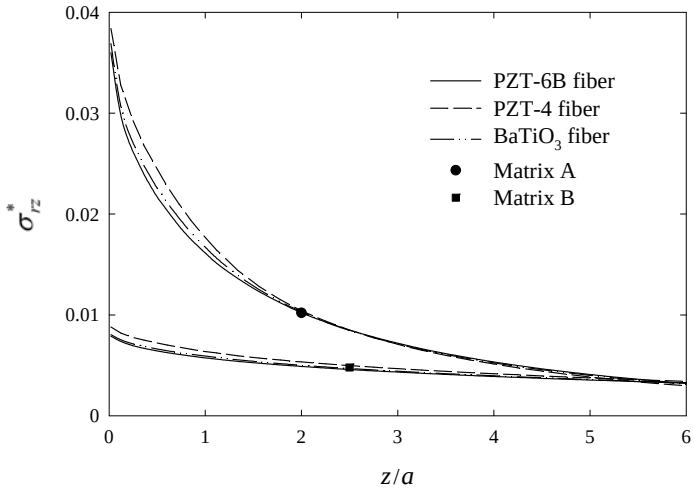

(a)

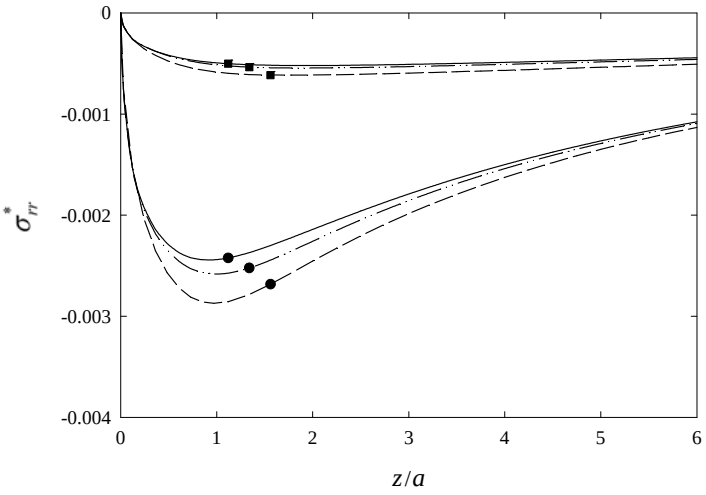

(b)

Figure 4.5 (a) Shear and (b) radial stresses along the fiber–matrix interface of piezoelectric composite (open-circuited) under applied axial load.

Next, consider the diffusion of a patch electric charge from a fiber perfectly bonded to a matrix. Nondimensional vertical stress, $\sigma_{zz}^{**} = \sigma_{zz}\, e_{15}^{f}\, a^2 / c_{44}^{f} Q_0$, and vertical electric field, $E_z^{**} = E_z\, (e_{15}^{f})^2\, a^2 / c_{44}^{f} Q_0$, along the *z*-axis are presented in Figures 4.6(a) and 4.6(b) respectively. A substantial dependence of vertical stress on the fiber type is noted. Vertical stress is zero at the loading plane and initially increases rapidly and then decreases slowly along the fiber axis. It is tensile along the upper fiber length, and PZT-4 has the highest nondimensional value. Figure 4.6(b) shows the variation of E_z^{**} along the fiber axis. In this case, $BaTiO_3$ and PZT–6B fibers have nearly equal but substantially smaller values of E_z^{**} when compared to a PZT-4 fiber. The decay of the vertical electric field along the fiber length is not rapid. Nondimensional shear stress, $\sigma_{rz}^{**} = \sigma_{rz}\, e_{15}^{f}\, a^2 / c_{44}^{f} Q_0$, and radial stress, $\sigma_{rr}^{**} = \sigma_{rr}\, e_{15}^{f}\, a^2 / c_{44}^{f} Q_0$, at the fiber-matrix interface due to an electric charge are shown in Figures 4.7(a) and 4.8(b) respectively. The variation of shear and radial stresses along the interface is somewhat similar to the results shown in Figure 4.5. However, the dependence of the interface stresses on the fiber and matrix material type is more pronounced in the case of electric charge loading when compared to the axial loading.

Figure 4.8 shows the resultant axial force and vertical electric field of a short-circuited fiber bonded to an elastic matrix due to an axial force P_0. The axial force profiles are similar to those shown in Figure 4.4(a) but the load transfer is slightly more rapid than the open-circuited case and the fiber properties have more influence on the force profiles. Vertical electric field decays very rapidly along the fiber length in contrast to Figure 4.4(b) and show less dependence on the matrix material. The interfacial stresses for the short-circuited case show behaviour similar to Figure 4.5 but the magnitudes are higher by 20-50%. Figure 4.9 shows the variation of vertical stress and vertical electric field when a short-circuited fiber is subjected to an electric charge Q_0. The profiles are very different from those shown in Figure 4.6 and show very rapid decay of axial stress and vertical electric field along the fiber length. The magnitudes show considerable dependence on the fiber

properties but negligible influence of matrix material. As in the case of Figure 4.6 the maximum nondimensional axial stress and vertical electric field values correspond to PZT-4. Comparisons with Figure 4.6 also show that axial stress and vertical electric field are much smaller in the short-circuited case.

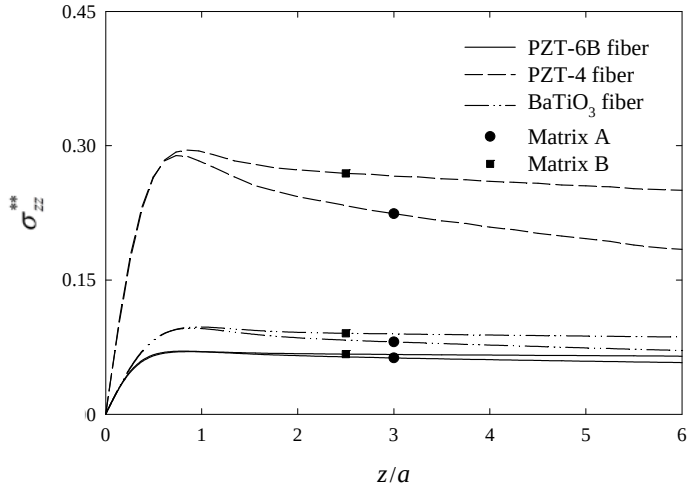

(a)

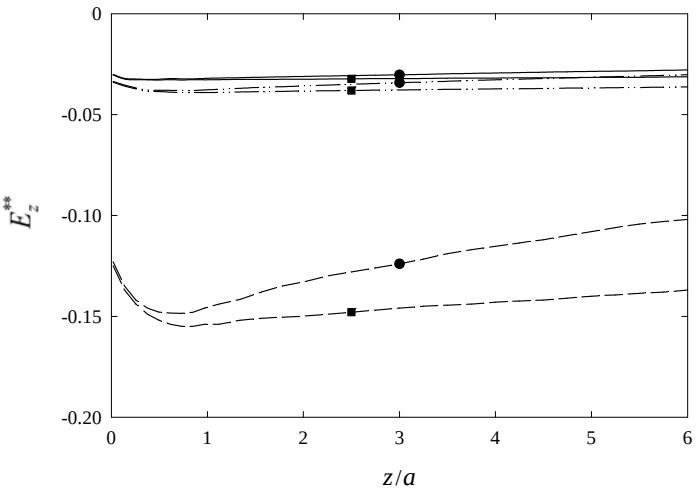

(b)

Figure 4.6 (a) Vertical stress and (b) vertical electric field along the *z*–axis of piezoelectric fiber (open-circuited) under applied electric charge.

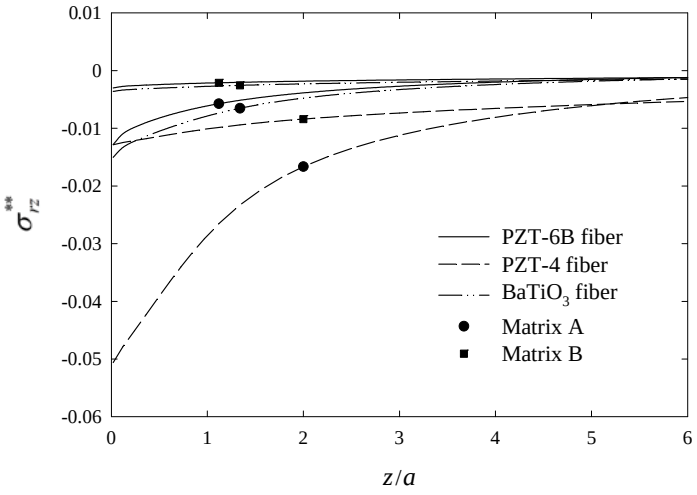

(a)

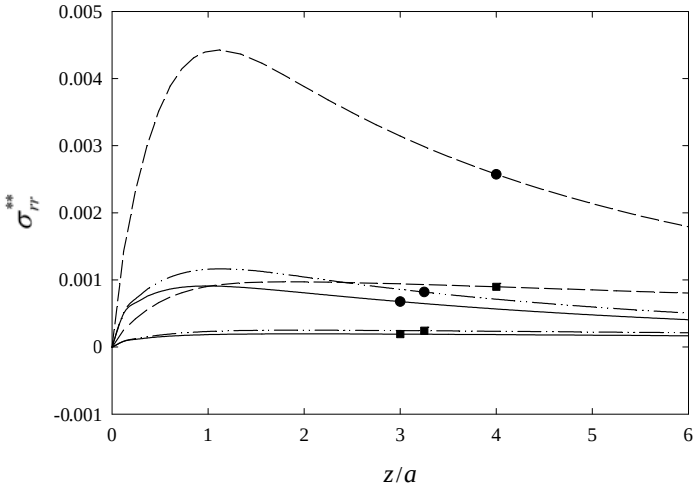

(b)

Figure 4.7 (a) Shear and (b) radial stresses along the fiber–matrix interface of piezoelectric composite (open-circuited) under applied electric charge.

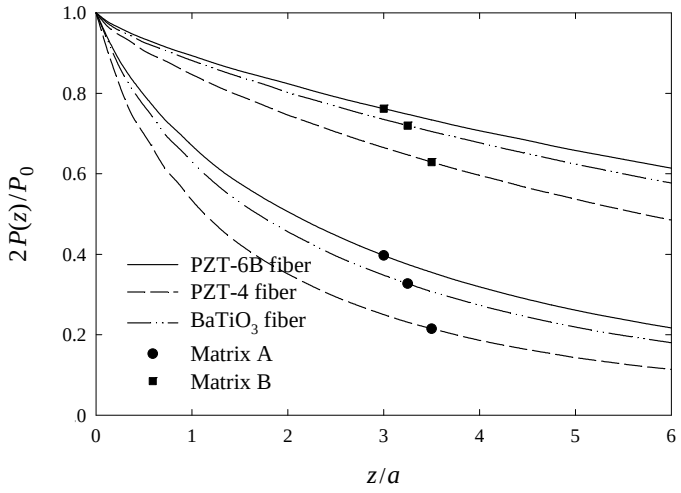

(a)

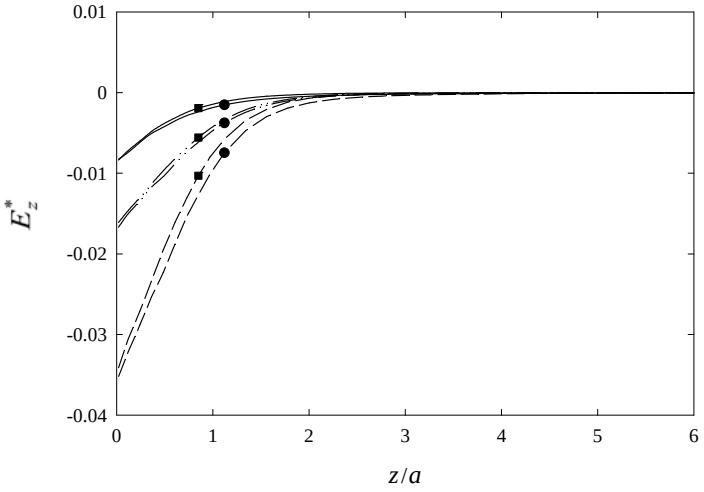

(b)

Figure 4.8 (a) Resultant axial force and (b) vertical electric field along the z–axis of piezoelectric fiber (short-circuited) under applied axial load.

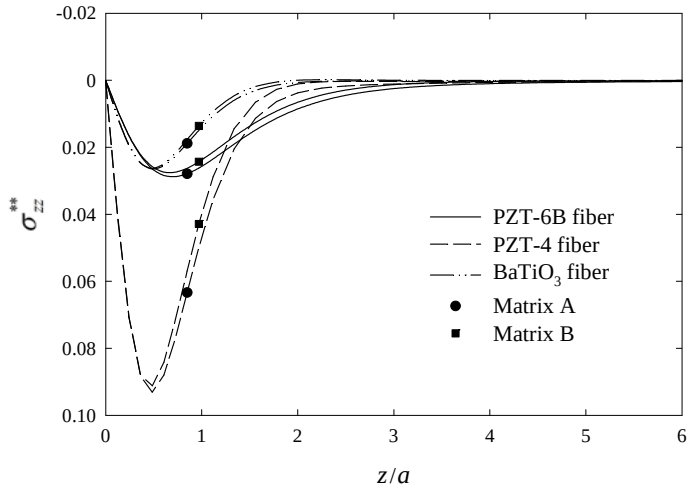

(a)

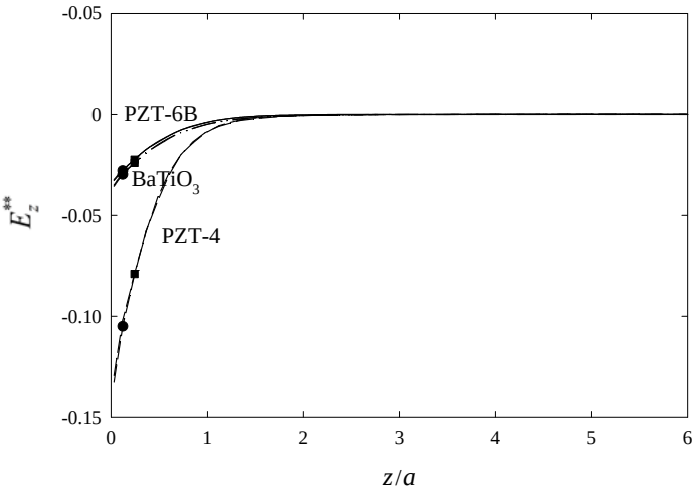

(b)

Figure 4.9 (a) Vertical stress and (b) vertical electric field along the z–axis of piezoelectric fiber (short-circuited) under applied electric charge.

The effect of imperfect fiber-matrix bonding on the load diffusion characteristics is presented in Figures 4.10-4.13. Two cases of piezocomposites are considered in the numerical study, i.e. composites of PZT-6B fiber with matrix A and PZT-4 fiber with matrix B. The interface behavior is characterized by the spring-factor model described in equation (4-3b). Five values of nondimensional spring-factor, $k_s^* = (k_s a)/c_{44}^f =$ 10, 1, 0.1, 0.01 and 0.001 are considered in the numerical study. Figures 4.10 and 4.11 show the electroelastic field of composites of PZT-6B fiber with matrix A and PZT-4 fiber with matrix B respectively under an applied axial load. Numerical results presented in Figures 4.10 and 4.11 demonstrate a substantial dependence of the electroelastic field of both composites on the interface stiffness. Figures 4.10(a) and 4.11(a) shows that fiber axial force significantly depends on the stiffness of the interface and as k^* decreases (weaker interface) the load transferred to the matrix is obviously reduced. The magnitudes of interfacial shear stress and radial stress obviously decrease as the interface bonding becomes weaker and the decay along the interface becomes less rapid. On the other hand, vertical electric field of the fiber increases in the case of a weaker interface due to less load transfer to the matrix. The magnitude of fiber vertical electric field can be considered a measure of the interface condition (weaker interface yields a higher fiber electric field). Therefore, it is possible to obtain a qualitative non-destructive assessment of the interface bond condition by comparing vertical electric field of fibers. A comparison of Figures 4.10 and 4.11 indicate that an imperfect interface has a relatively lesser effect on the load diffusion in a PZT-4/Matrix B composite and the interfacial stresses are also smaller.

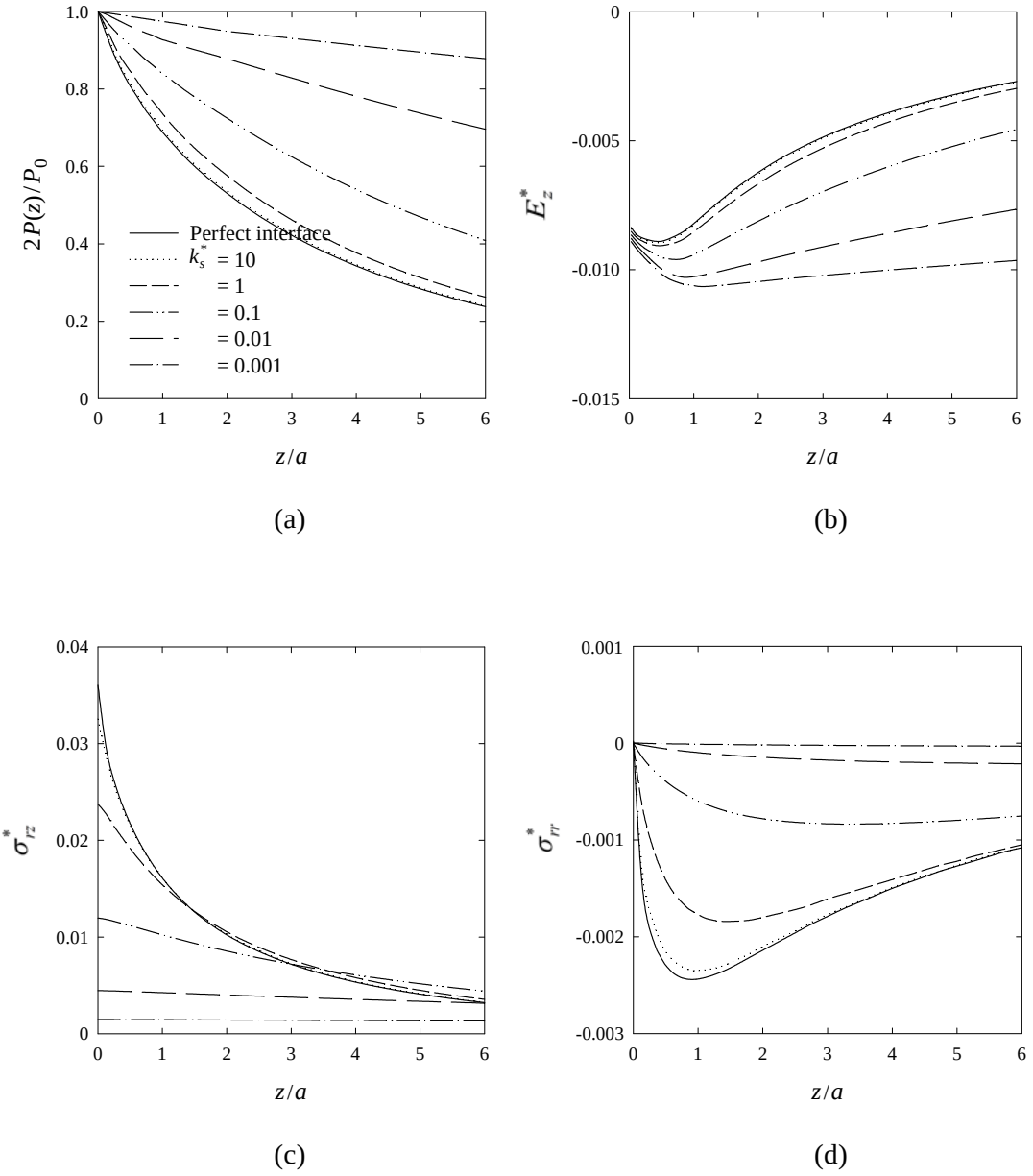

Figure 4.10 Composite of PZT-6B fiber with Matrix A (a) resultant axial force and (b) vertical electric field along the *z*–axis of piezoelectric fiber; (c) shear and (d) radial stresses along the fiber–matrix interface (open-circuited) under applied axial load for different interface stiffness values.

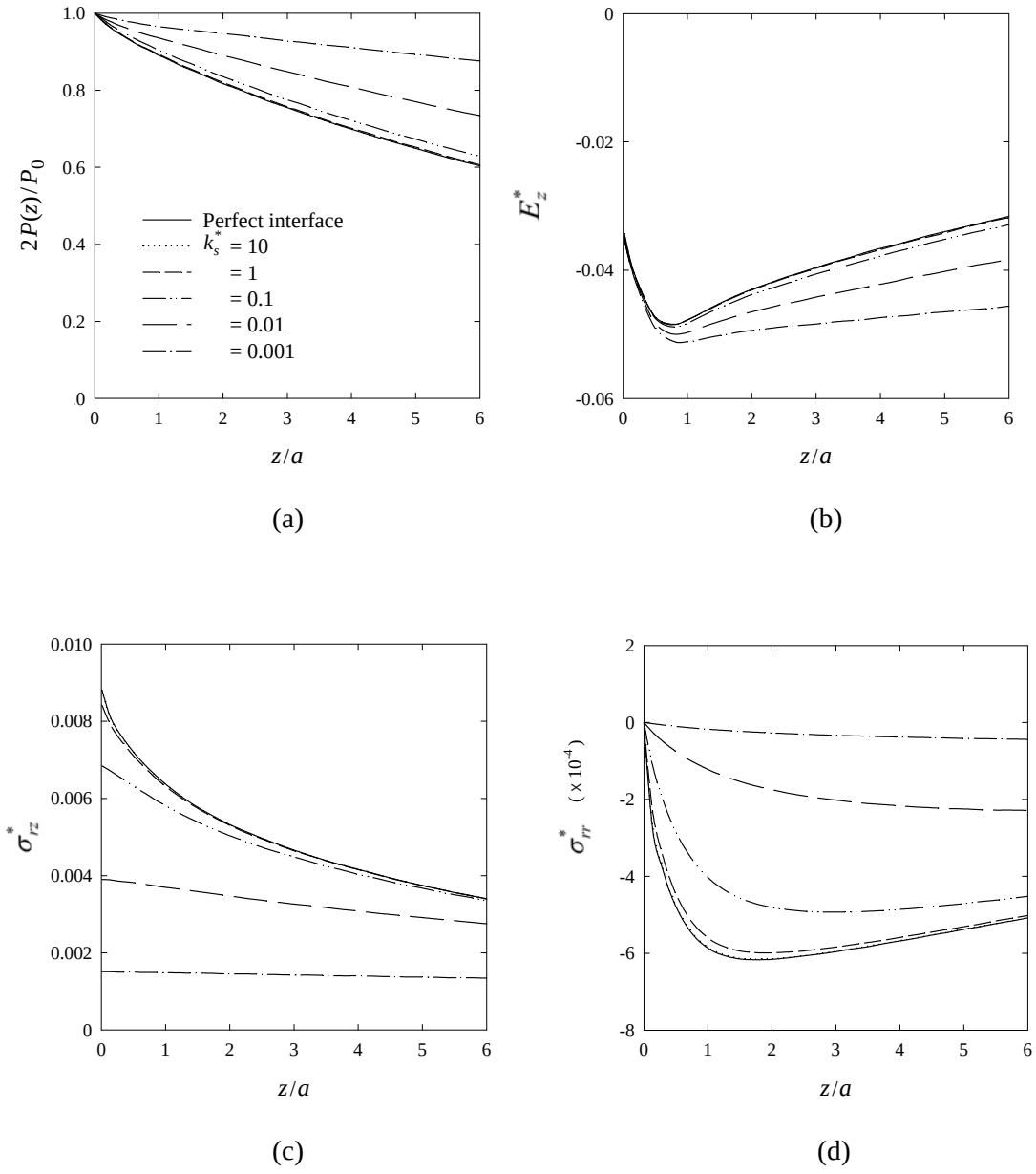

Figure 4.11 Composite of PZT-4 fiber with Matrix B (a) resultant axial force and (b) vertical electric field along the z–axis of piezoelectric fiber; (c) shear and (d) radial stresses along the fiber–matrix interface (open-circuited) under applied axial load for different interface stiffness values.

The effect of an imperfect interface on electric charge transfer is shown in Figure 4.12 for a composite of PZT-6B fibers with matrix A and in Figure 4.13 for a composite of PZT-4 fibers with matrix B. The influence of interface bonding condition is relatively small when compared to the effects observed in Figures 4.10 and 4.11 for an axial load. Vertical electric field is negative and its absolute value is increased as the interface becomes weaker. The fiber tensile axial stress is also increased as the interface becomes weaker. However, near the loading plane vertical stress and electric field show negligible influence of the interface stiffness. Nondimensional shear and radial stresses indicate that interfacial stresses decrease as the interface becomes weaker similar to the behavior observed for the axial load diffusion but the stresses have signs opposite to those corresponding to the axial load transfer case. A comparison of Figures 4.12 and 4.13 shows that the influence of interface stiffness is less in the case of PZT-4/Matrix B composites under electric charge loading similar to the case of axial loading.

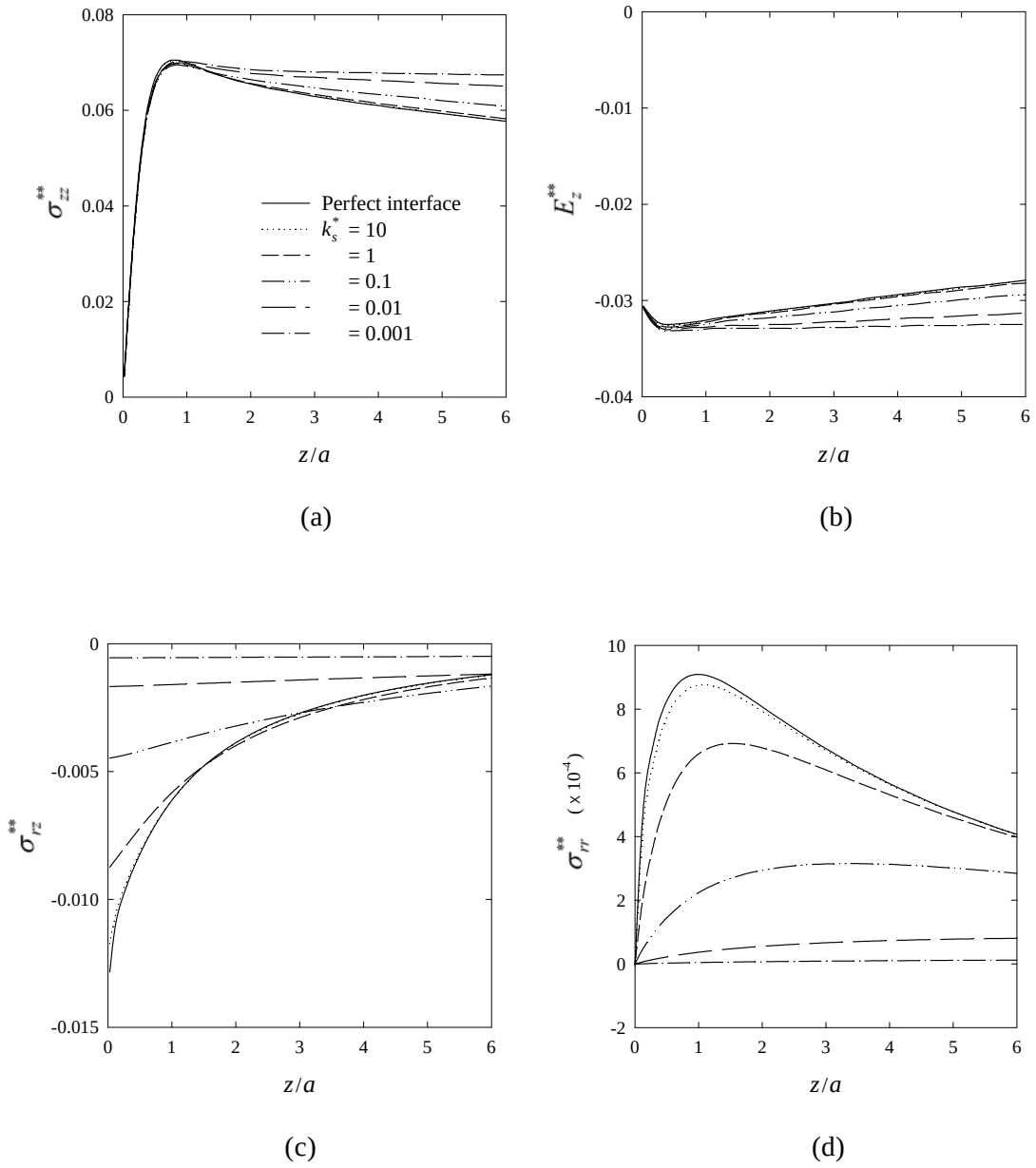

Figure 4.12 Composite of PZT-6B fiber with Matrix A (a) vertical stress and (b) vertical electric field along the z–axis of piezoelectric fiber; (c) shear and (d) radial stresses along the fiber–matrix interface of piezoelectric composite (open-circuited) under applied electric charge for different interface stiffness values.

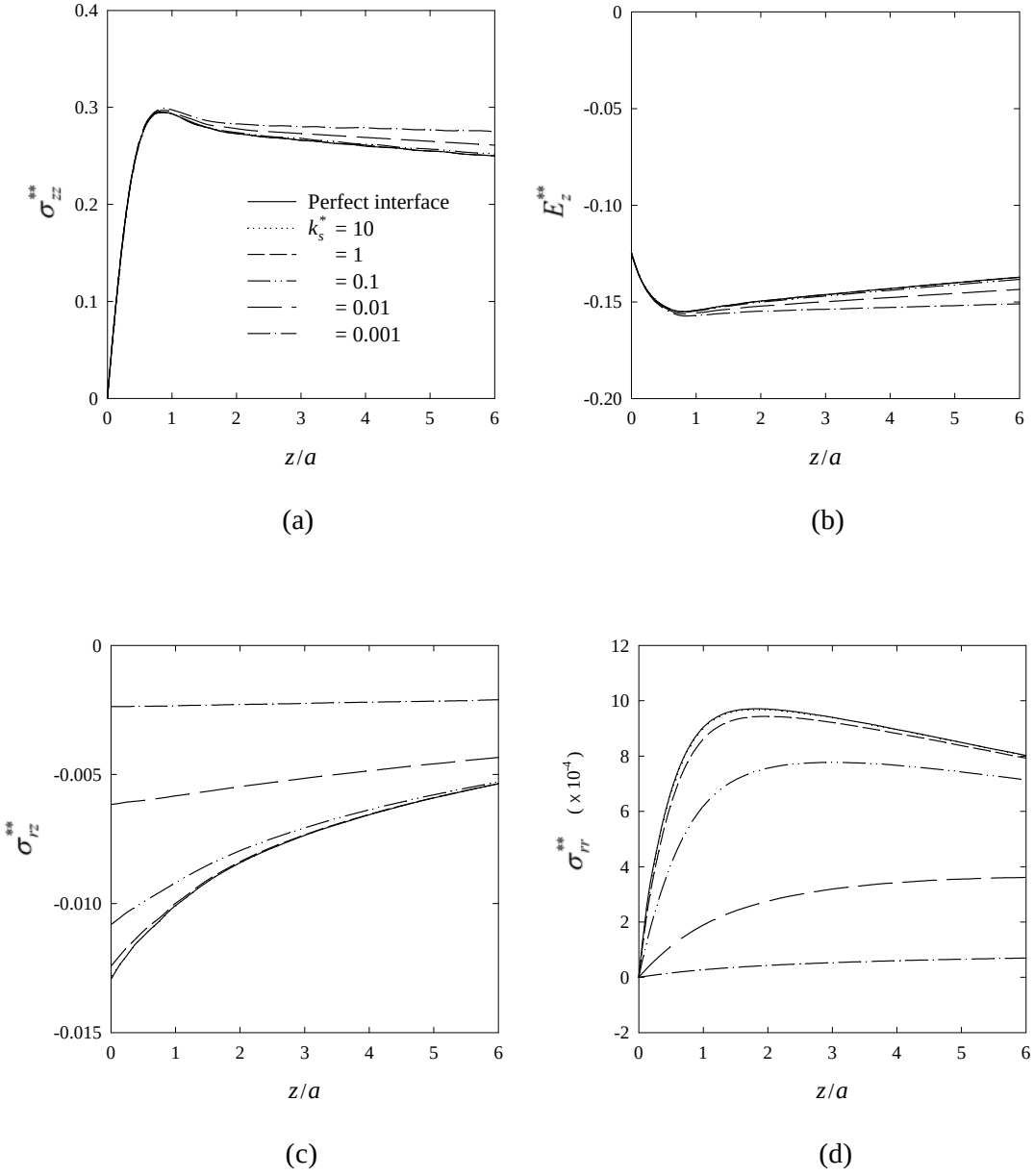

Figure 4.13 Composite of PZT-4 fiber with Matrix B (a) vertical stress and (b) vertical electric field along the z–axis of piezoelectric fiber; (c) shear and (d) radial stresses along the fiber–matrix interface of piezoelectric composite (open-circuited) under applied electric charge for different interface stiffness values.

CHAPTER V

INTERFACIAL CRACKS IN PIEZOCOMPOSITES

In this chapter, three-dimensional axisymmetric interfacial cracks in a 1-3 piezoelectric fiber-reinforced composite are examined by adopting the displacement discontinuity method (DDM) based on the fundamental solutions of elemental constant displacement discontinuity. The general solutions of piezoelectric fiber and elastic matrix presented in chapter 3 are used to derive the required fundamental solutions. A special crack tip element is introduced in the DDM formulation for modeling the accuracy of the field quantities in the vicinity of the crack tips. The mathematical implementation and the extended field intensity factors for piezoelectric material and interface crack in piezocomposite are discussed.

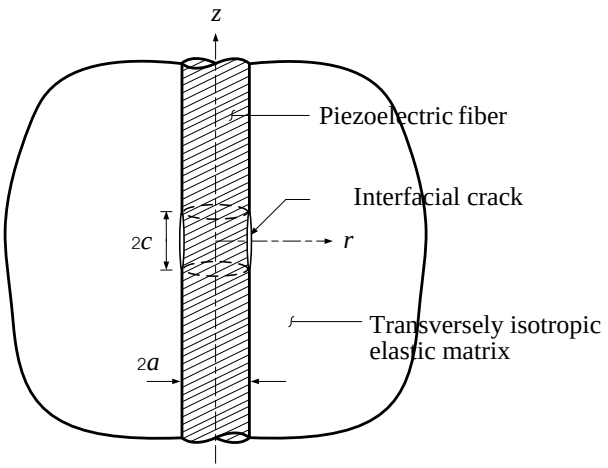

Figure 5.1 Piezoelectric fiber-reinforced composite with interfacial crack.

5.1 PROBLEM FORMULATION

Consider a piezocomposite that consists of a cylindrical piezoelectric fiber of radius "*a*" perfectly bonded to a transversely isotropic elastic matrix but contains a cylindrical interfacial crack of lengh "2*c*" as shown in Figure 5.1. The condition along the fiber–matrix interface is assumed to be electrically impermeable. The

displacement discontinuity method (DDM) is employed for the analysis of this fracture problem. The DDM analysis of the interfacial crack requires the fundamental solutions for elemental radial and tangential displacement discontinuities at the fiber-matrix interface of in a piezocomposite as shown in Figure 5.2. Details on the derivation of the fundamental solutions and the DDM formulation are given in the subsequent sections.

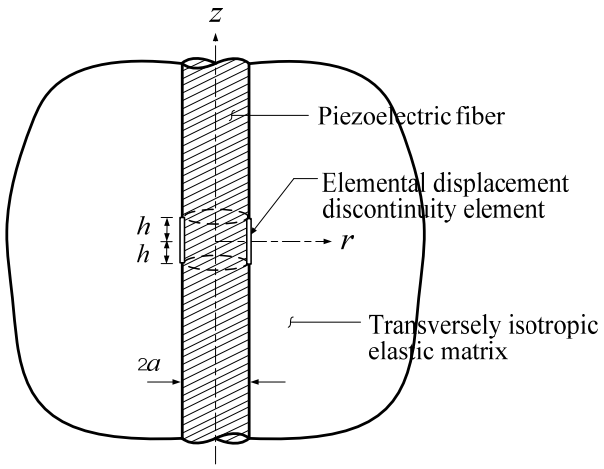

Figure 5.2 Piezocomposite with an elemental displacement discontinuity element.

5.1.1 Fundamental Solutions for Elemental Displacement Discontinuity

5.1.1.1 Radial Displacement Discontinuity

Consider a piezoelectric fiber-reinforced composite with constant radial displacement discontinuity, d_r, of a finite cylindrical region with radius "a" and length "$2h$" at the fiber-matrix interface (Figure 5.2). The fiber–matrix interface is assumed to be electrically impermeable and perfectly bonded. The boundary and continuity conditions along the fiber-matrix interface ($r = a$) can be expressed as

Displacement continuity

$$u_r^f(a,z) - u_r^m(a,z) = d_r \left[H(z+h) - H(z-h)\right] \tag{5-1a}$$

$$u_z^f(a,z) - u_z^m(a,z) = 0 \tag{5-1b}$$

Stress continuity

$$\sigma_{rr}^{f}(a,z) - \sigma_{rr}^{m}(a,z) = 0 \tag{5-1c}$$

$$\sigma_{rz}^{f}(a,z) - \sigma_{rz}^{m}(a,z) = 0 \tag{5-1d}$$

Electrical boundary condition

$$D_{r}^{f}(a,z) = 0 \tag{5-1e}$$

where H(.) denotes the Heaviside step function. Noted that the superscripts "*f*" and "*m*" are used to identify the quantities corresponding to the fiber ($0 \le r \le a$) and matrix ($a \le r < \infty$) respectively.

The general solutions of piezoelectric fiber and elastic matrix are expressed by equation (3-18) with arbitrary functions A_1, A_2 and A_3 and equation (3-19) with arbitrary C_1 and C_2 respectively. Application of Fourier integral transform to equation (5-1) and the substitution of general solutions result in the following solutions for arbitrary functions A_1, A_2, A_3, C_1 and C_2:

$$A_1 = d_r \left\{ I_{a1} h_{a1} \gamma_1 + [I_{a1} p_{a1} + h_{b1}(I_{b1} + I_{c1})]\gamma_2 + p_{b1}(I_{a1} + I_{b1})\gamma_2 \right\} / W \tag{5-2a}$$

$$A_2 = -d_r \left\{ I_{a2} h_{a2} \gamma_1 + [I_{a2} p_{a2} + h_{b2}(I_{b2} + I_{c2})]\gamma_2 + p_{b2}(I_{a2} + I_{b2})\gamma_2 \right\} / W \tag{5-2b}$$

$$A_3 = d_r \left\{ I_{a3} h_{a3} \gamma_1 + [I_{a3} p_{a3} + h_{b3}(I_{b3} + I_{c3})]\gamma_2 + p_{b3}(I_{a3} + I_{b3})\gamma_2 \right\} / W \tag{5-2c}$$

$$C_1 = d_r \left\{ K_{02} n_2 (\gamma_4 + \gamma_5) + (s_2 K_{12} + |\xi| y_{12} K_{02})\gamma_6 \right\} / W \tag{5-2d}$$

$$C_2 = -d_r \left\{ K_{01} n_1 (\gamma_4 + \gamma_5) + (s_1 K_{11} + |\xi| y_{11} K_{01})\gamma_6 \right\} / W \tag{5-2e}$$

where

$$\begin{aligned} W = \beta_1 \Big[& \left\{ K_{02} K_{11} n_2 s_1 - K_{01} K_{12} n_1 s_2 + |\xi| K_{01} K_{02} (n_2 y_{11} - n_1 y_{12}) \right\} \\ & + \beta_1 K_{02} K_{11} n_2 y_{11} - \beta_2 K_{01} K_{12} n_1 y_{22} + |\xi| \gamma_6 K_{11} K_{12} (s_2 w_1 - s_1 w_2) \\ & + |\xi|^2 \gamma_6 \left\{ K_{01} K_{12} w_2 y_{11} - K_{02} K_{11} w_1 y_{12} + K_{11} K_{12} (w_2 y_{21} - w_1 y_{22}) \right\} \\ & + |\xi| \left\{ (\gamma_4 + \gamma_5)(K_{02} K_{11} n_2 w_1 - K_{01} K_{12} n_1 w_2 + \right\} \Big] / (\sqrt{2/\pi} \sin(\xi h) / \xi) \end{aligned} \tag{5-3a}$$

and

$$I_{mj} = I_m(\xi_j a); \quad K_{mk} = K_m(\xi_k a); \ (m = 0,1;\ j = 1,2,3;\ k = 1,2) \tag{5-3b}$$

$$h_{1j} = c_{11}^f v_j - c_{13}^f k_{1j} - e_{13}^f k_{2j}\,; \quad h_{2j} = i\xi_j \left[c_{44}^f (1+k_{1j}) - e_{15}^f k_{2j} \right]$$

$$h_{3j} = i\xi_j \left[e_{15}^f (1+k_{1j}) - d_{11}^f k_{2j} \right]; \; g_j = \nu_j (c_{12}^f - c_{11}^f)/a\,; \quad m_j = k_{1j}^h \tag{5-3c}$$

$$y_{1k} = c_{11}^m w_k - c_{13}^m n_k\,; \quad s_k = w_j (c_{12}^m - c_{11}^m)/a$$

$$I_{a1} = I_{12} I_{13}\,; \; I_{a2} = I_{11} I_{13}\,; \; I_{a3} = I_{11} I_{12} \; I_{b1} = I_{03} I_{12}\,; I_{b2} = I_{03} I_{11}$$

$$I_{b3} = I_{02} I_{11}\,; \; I_{c1} = I_{02} I_{13}\,; \quad I_{c2} = I_{01} I_{13}\,; \quad I_{c3} = I_{01} I_{12} \tag{5-3d}$$

$$I_{d1} = I_{01} I_{12} I_{13}\,; \; I_{d2} = I_{02} I_{11} I_{13}\,; \; I_{d3} = I_{03} I_{11} I_{12}\,; \; I_e = I_{11} I_{12} I_{13}$$

$$K_a = K_{02} K_{11}\,; \quad K_b = K_{01} K_{12}\,; \; K_c = K_{01} K_{02}\,; \; K_d = K_{11} K_{12}$$

$$h_{a1} = h_{22} h_{33} - h_{23} h_{32}\,; \quad h_{a2} = h_{21} h_{33} - h_{23} h_{31}\,; \quad h_{a3} = h_{21} h_{32} - h_{22} h_{31}$$

$$h_{b1} = h_{12} h_{33} - h_{13} h_{32}\,; \quad h_{b2} = h_{11} h_{33} - h_{13} h_{31}\,; \quad h_{b3} = h_{11} h_{32} - h_{12} h_{31} \tag{5-3e}$$

$$p_{a1} = g_2 h_{33} - g_3 h_{32}\,; \quad p_{a2} = g_1 h_{33} - g_3 h_{31}\,; \quad p_3 = g_1 h_{32} - g_2 h_{31}$$

$$p_{b1} = m_2 h_{33} - m_3 h_{32}\,; \quad p_{b2} = m_1 h_{33} - m_3 h_{31}\,; \quad p_{b3} = m_1 h_{32} - m_2 h_{31} \tag{5-3f}$$

$$p_{c1} = g_2 h_{23} - g_3 h_{22}\,; \quad p_{c2} = g_1 h_{23} - g_3 h_{21}\,; \quad p_{c3} = g_1 h_{22} - g_2 h_{21}$$

In addition, the parameters γ_i and β_i are defined by

$$\gamma_1 = K_a n_2 s_1 - K_b n_1 s_2 + |\xi| K_c (n_2 y_{11} - n_1 y_{12}) + I_{02} I_{01} I_{13} h_{23} (k_{12} h_{11} - k_{11} h_{12}) \tag{5-4a}$$

$$\gamma_2 = n_2 y_{21} K_a - |\xi| n_1 y_{22} K_b \tag{5-4b}$$

$$\gamma_3 = (s_2 y_{21} - s_1 y_{22}) K_d + |\xi| (y_{12} y_{21} K_a - y_{11} y_{22} K_b) \tag{5-4c}$$

$$\gamma_4 = |\xi| (h_{11} h_{a1} I_{d1} + h_{12} h_{a2} I_{d2} + h_{13} h_{a3} I_{d3}) \tag{5-4d}$$

$$\gamma_5 = I_e (h_{31} p_{c1} + h_{32} p_{c2} + h_{33} p_{c3}) \tag{5-4e}$$

$$\gamma_6 = I_{d1} m_1 h_{a1} + I_{d2} m_2 h_{a2} + I_{d3} m_3 h_{a3} \tag{5-4f}$$

$$\gamma_7 = |\xi| (K_a w_1 z_{12} - K_b w_2 z_{11}) + K_d (s_2 w_1 - s_1 w_2) \tag{5-4g}$$

$$\gamma_8 = (h_{33} v_2 - h_{32} v_3) \left[|\xi| (z_{12} z_{21} K_a - z_{11} z_{22} K_b) + K_d (s_2 z_{21} - s_1 z_{22}) \right] \tag{5-4h}$$

$$\beta_1 = |\xi| I_e (h_{a1} v_1 + h_{a2} v_2 + h_{a3} v_3) \tag{5-4i}$$

$$\beta_2 = |\xi| I_e (p_{a1} v_1 + p_{a2} v_2 + p_{a3} v_3) \tag{5-4j}$$

5.1.1.2 Tangential Displacement Discontinuity

The boundary and continuity conditions along the fiber-matrix interface ($r = a$) for the case of elemental tangential displacement discontinuity (Figure 5.2) can be expressed as

Displacement continuity

$$u_z^f(a,z) - u_z^m(a,z) = d_z\left[H(z+h) - H(z-h)\right] \tag{5-5a}$$

$$u_r^f(a,z) - u_r^m(a,z) = 0 \tag{5-5b}$$

Stress continuity

$$\sigma_{rr}^f(a,z) - \sigma_{rr}^m(a,z) = 0 \tag{5-5c}$$

$$\sigma_{rz}^f(a,z) - \sigma_{rz}^m(a,z) = 0 \tag{5-5d}$$

Electrical boundary condition

$$D_r^f(a,z) = 0 \tag{5-5e}$$

A procedure identical to the case of radial displacement discontinuity results in the following solutions for arbitrary functions A_1, A_2, A_3, C_1 and C_2:

$$A_1 = d_z\left\{|\xi| I_{a1}(h_{a1}\gamma_7 + \gamma_8) + k_d(w_1 y_{22} - w_2 y_{21})[|\xi| I_{a1} p_{a1} + (I_{b1} + I_{c1})h_{b1}]\right\}/W \tag{5-6a}$$

$$A_2 = -d_z\left\{|\xi| I_{a2}(h_{a2}\gamma_7 + \gamma_8) + k_d(w_1 y_{22} - w_2 y_{21})[|\xi| I_{a2} p_{a2} + (I_{b2} + I_{c2})h_{b2}]\right\}/W \tag{5-6b}$$

$$A_3 = d_z\left\{|\xi| I_{a3}(h_{a3}\gamma_7 + \gamma_8) + k_d(w_1 y_{22} - w_2 y_{21})[|\xi| I_{a3} p_{a3} + (I_{b3} + I_{c3})h_{b3}]\right\}/W \tag{5-6c}$$

$$C_1 = d_z\left\{|\xi| K_{12} w_2(\gamma_4 + \gamma_5) + (K_{12} s_2 + |\xi| K_{02} y_{12})\beta_1 + K_{12} y_{22}\beta_2\right\}/W \tag{5-6d}$$

$$C_2 = -d_z\left\{|\xi| K_{11} w_1(\gamma_4 + \gamma_5) + (K_{11} s_1 + |\xi| K_{01} y_{11})\beta_1 + K_{11} y_{21}\beta_2\right\}/W \tag{5-6e}$$

5.1.2 The Displacement Discontinuity Method (DDM)

The displacement discontinuity method (DDM), introduced by Crouch and Starfield [44] for cracks in plane elasticity, is further adopted for analysis of interfacial cracks in piezocomposite (Figure 5.1). The DDM subdivides the crack surface into *N* segments as shown in Figure 5.3. Each segment represents an

elemental displacement discontinuities in r- and z- directions and its components, d_r and d_z, are defined by

$$d_r = u_r^f(a,z) - u_r^m(a,z) \tag{5-7a}$$

$$d_z = u_z^f(a,z) - u_z^m(a,z) \tag{5-7b}$$

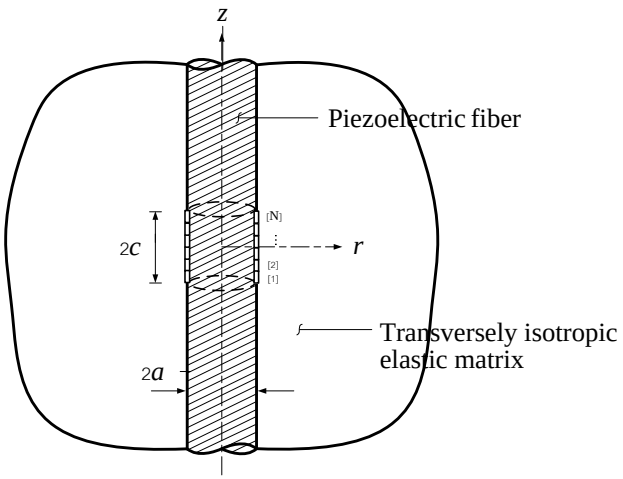

Figure 5.3 Discretization of crack surface into *N* segments.

The influence of a single displacement discontinuity from each element on the displacements and stresses at an arbitrary point in the composite material can be determined. In particular, the radial and tangential stresses at the midpoint of the *i*th element can be expressed in terms of the displacement discontinuity components at the *j*th element as

$$\left.\begin{aligned} \sigma_{rr}^i &= A_{rr}^{ij} d_r^j + A_{rz}^{ij} d_z^j \\ \sigma_{rz}^i &= A_{zr}^{ij} d_r^j + A_{zz}^{ij} d_z^j \end{aligned}\right\} \; i, j = 1, 2, ..., N \tag{5-8}$$

where A_{rr}^{ij}, A_{rz}^{ij}, A_{zr}^{ij} and A_{zz}^{ij} are the influence coefficients for the stresses along the fiber–matrix interface. For example, the coefficient A_{zr}^{ij} denotes the interfacial tangential stress at the midpoint of the *i*th element due to a constant unit radial displacement discontinuity (d_r = 1) over the *j*th element. These influence

coefficients can be obtained from the fundamental solutions of elemental displacement discontinuities.

The specified values of the radial and tangential stresses for each element, σ_{rr}^{i} and σ_{rz}^{i}, leads to a system of 2*N* linear equations for 2*N* unknowns, which are the elemental displacement discontinuity components d_r^i and d_z^i. After solving the above equations for d_r^i and d_z^i (i = 1, 2, …, *N*), the displacements, stresses and electric field at designated points in the composite material can be determined from the fundamental solutions, given by equation (3-17) for the piezoelectric fiber and equation (3-18) for the elastic matrix respectively, together with the principle of superposition.

5.1.3 Crack tip element

The modeling of a crack tip is an important key for the determination of field intensity factors in fracture mechanics. A corollary of the $r^{-1/2}$ variation in stress near the crack tip is that the relative displacement between the crack surfaces is proportional to $r^{1/2}$ close to the tip, where *r* is measured from the tip along the crack. This requirement encourages us to introduce a special element at the crack tip to replace a constant displacement discontinuity element. The schematic of the crack tip displacement discontinuity element is shown in Figure 5.4 and the displacement discontinuity functions for a special crack tip element used in the present model can be expressed by

$$\hat{u}_i(z) = u_i^f(a,z) - u_i^m(a,z) = d_i(z/a)^{1/2}, \quad 0 \le z \le 2h, \quad i = r,z \tag{5-9}$$

where $\hat{u}_i\,(i = r,z)$ is the relative displacement between the crack surface and 2*h* is the length of the crack tip element.

The fundamental solution corresponding to the crack tip displacement discontinuity functions can be determined by replacing the first condition of equation (5-1a) by equation (5-9) and solving the relevant boundary-value problem. The crack tip element is implemented in the DDM formulation at each end of the

discretized element by substituting the influence coefficients, A_{rr}^{ij}, A_{rz}^{ij}, A_{zr}^{ij} and A_{zz}^{ij}, in equation (5-8) by the corresponding crack tip influence functions for i = 1 and i = N.

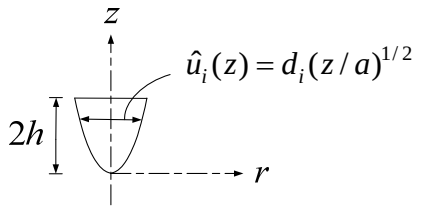

Figure 5.4 Displacement discontinuity element at the crack tip.

5.1.4 Extended Field Intensity Factors

The field intensity factor is an important concept in fracture mechanics. This invariant nature of the crack tip stresses reduces the analysis to the determination of the intensity factors for the specific problem of interest. Analytical solutions to the problem of crack in a homogeneous material show that the stress fields in the neighborhood of a crack tip have square root singularities. The interface cracks in bimaterials may contain singularity beside the classical square root. The order of singularity for the interface crack can be determined by using Stroh's formulation [54] or Lekhnitskii's approach [55]. It is noted that the order of singularity for the crack can be determined by using any orthogonal coordinate system and the axisymmetric crack and the plane crack at the same interface of bimaterials then have the same characteristics of singularity.

Based on Stroh's formulation, Suo et al. [38] derived the solution for plane problem of an impermeable interface crack in general anisotropic piezoelectric bimaterials in the form

$$h(z) = \mathbf{w} z^{-1/2+i\gamma} \tag{5-10}$$

which satisfies the Hilbert problem

$$\bar{\mathbf{H}}\mathbf{w} = e^{2\pi\gamma}\mathbf{H}\mathbf{w} \tag{5-11}$$

where $\mathbf{H}$ depends upon the material constants.

The Hilbert problem of equation (5.11) can be reduced to the eigenvalue problem given by

$$(\mathbf{D}^{-1}\mathbf{W}+i\beta\mathbf{I})\mathbf{w}=0\,,\quad \left\|\mathbf{D}^{-1}\mathbf{W}+i\beta\mathbf{I}\right\|\mathbf{w}=\beta^4+2b\beta+c=0 \tag{5-12a}$$

$$\gamma=-[\tanh^{-1}(\beta)]/\pi\,,\quad b=\left\{tr\left[(\mathbf{D}^{-1}\mathbf{W})^2\right]\right\}/4\,,\quad c=\left\|\mathbf{D}^{-1}\mathbf{W}\right\| \tag{5-12b}$$

$$\mathbf{D}=\mathrm{Re}[\mathbf{H}],\quad \mathbf{W}=\mathrm{Im}[\mathbf{H}],\quad \mathbf{H}=\mathbf{Y}_1+\bar{\mathbf{Y}}_2\,,\quad \mathbf{Y}=i\mathbf{A}\mathbf{B}^{-1} \tag{5-12c}$$

The matrices $\mathbf{A}$ and $\mathbf{B}$ depend upon the material constants. Denoting the real and imaginary roots of the characteristic equation (5.10) by $\pm\varepsilon$ and $\pm\kappa$ respectively, where both ε and κ are real numbers and expressing them by

$$\varepsilon=\left\{\tanh^{-1}\left[(b^2-c)^{1/2}-b\right]^{1/2}\right\}/\pi\,,\quad \kappa=\left\{\tanh^{-1}\left[(b^2-c)^{1/2}+b\right]^{1/2}\right\}/\pi \tag{5-13}$$

With four distinct eigenvalues ε, $-\varepsilon$, $i\kappa$, $-i\kappa$ and four linearly independent eigenvectors w_1, $\bar{w}_1$, w_3, w_4, in which w_3 and w_4 are real vectors, the solution can be written as

$$\mathbf{h}(z)=h_1\mathbf{w}_1z^{-1/2+i\varepsilon}+h_2\bar{\mathbf{w}}_1z^{-1/2-i\varepsilon}+h_3\mathbf{w}_3z^{-1/2-\kappa}+h_4\mathbf{w}_4z^{-1/2+\kappa} \tag{5-14}$$

where h_1, h_2, h_3 and h_4 are arbitrary complex constants. The crack-tip stress field can then be obtained as

$$[\sigma_{2i}]=[\sigma_{21},\sigma_{22},\sigma_{23},D_2]=2\,\mathrm{Re}[\mathbf{h}(z)] \tag{5-15}$$

A reduced class from the generalized anisotropic piezoelectric materials is the transversely isotropic piezoelectric (TIP) materials, which is more practical significance, because almost all piezoelectric materials commercially used today can be classified into this category. For the interface crack perpendicular to the poling direction of TIP bimaterials, it has been shown that one of the two parameters ε and κ vanishes [48, 49]. When the order of stress singularity is such that $\varepsilon\neq 0$, the

displacement becomes oscillatory near r = 0 and the two crack surfaces penetrate each other. This is a physically unacceptable phenomenon, although the region of penetration is rather small. There have been several studies on the problem to eliminate the unrealistic oscillatory phenomenon by introducing a contact zone near the crack tip [56, 57]. Nevertheless, the calculation show that the singularity indices ε and κ for interface crack at a piezoelectric composite are relatively small compared to the classical 1/2 singularity [48, 49]. The classical square root singularity is therefore the dominate term for an interface crack and the singularity index ε and κ can be treated as zero for practical applications.

It should be noted that not all inteface cracks have the interpenetration problem. By considering equations (5.12)-(5.13), ε=0 if $\mathbf{W} = \mathbf{0}$ or $\mathbf{H}$ is real. The non-complex (ε=0) singularity for interface crack happens when some conditions or symmetry are met. For interface crack in isotropic bimaterial, the non-complex singularity occurs when the value of (1-2ν)/μ for the two materials are identical [58]. It can be proved that the interface crack parallel to the principal material direction has a classical (non-complex) singularity [38, 40]. The extended field intensity factors for the axisymmetric cylindrical crack at the interface of piezocomposite for the present study can then be defined by

$$K_I = \lim_{z \to c} \sqrt{2\pi(z-c)}\,(\sigma_{rr})\Big|_{r=a} \tag{5-16a}$$

$$K_{II} = \lim_{z \to c} \sqrt{2\pi(z-c)}\,(\sigma_{rz})\Big|_{r=a} \tag{5-16b}$$

$$K_D = \lim_{z \to c} \sqrt{2\pi(z-c)}\,(D_r)\Big|_{r=a} \tag{5-16c}$$

Noted that the mode III deformation vanishes for the axisymmtric crack problem. A comprehensive treatment of electroelastic singularities in multi-material wedges and junctions for piezoelectric and elastic anisotropic solids can be found in Xu and Rajapakse [40].

5.2 NUMERICAL SOLUTIONS

5.2.1 Numerical Scheme

A computer code based on the DDM formulation presented in the preceding section has been developed to study the problem of interface cracks in piezocomposites (Figure 5.1). The required influence functions for the interface dislocation are obtained by evaluating the inverse Fourier integral transform, defined in equation (3-9b), with respect to ξ. A globally adaptive numerical quadrature scheme is employed to evaluate the integrals. For the purpose of numerical evaluation, the modified Bessel functions $I_n(x)$ and $K_n(x)$ appeared in the integrand are evaluated by using the scaled modified Bessel functions $\hat{I}_n(x)$ and $\hat{K}_n(x)$ defined by [59]

$$\hat{I}_n(x) = e^{-x} I_n(x); \quad \hat{K}_n(x) = e^{x} K_n(x) \tag{5-17}$$

The validity and accuracy of the present formulation is first verified by comparing with the solutions reported by Kasano et al. [31] for a cylindrical crack in a transversely isotropic elastic body. Their results correspond to a constant pressure on the crack surfaces for E.glass/epoxy and graphite/epoxy composites and isotropic material with the elastic constants given in Table 5.1 where E, G and ν represent the longitudinal and transverse moduli and Poisson's ratio in the plane of isotropic, respectively, while E', G' and ν' are the corresponding properties in the principal material direction. A material with same elastic properties as Kasano et al. [31] is selected and the piezoelectric constants are set to negligibly small values in the present scheme.

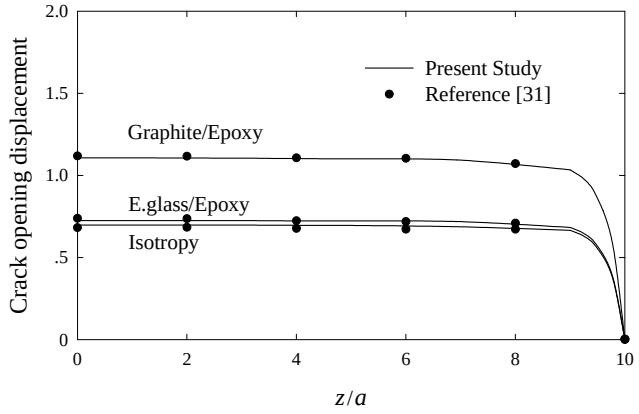

(a) $c/a = 10$

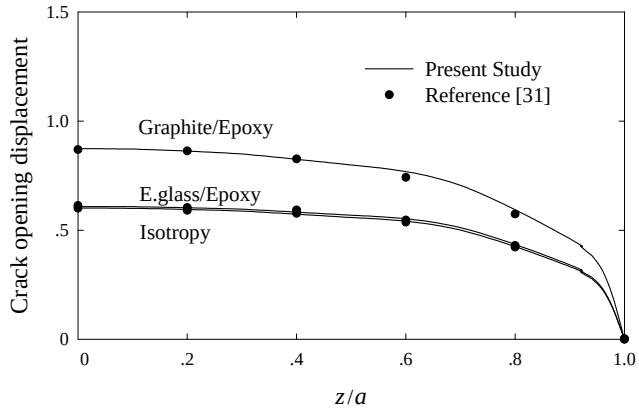

(b) $c/a = 1$

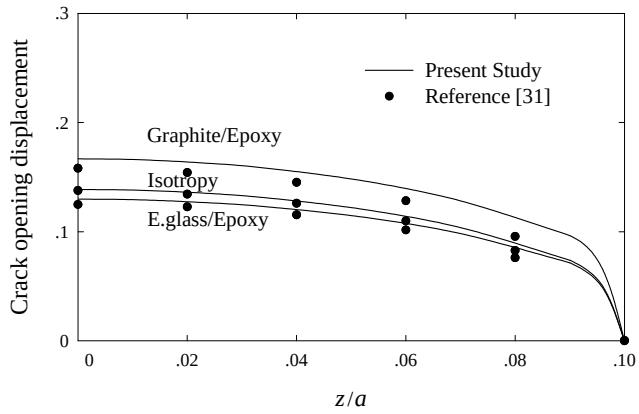

(c) $c/a = 0.1$

Figure 5.5 Comparison of crack opening displacement for cylindrical crack in elastic materials.

Table 5.1 Material properties used by Kasano et al. [31]

	E'/E	G'/G	ν	ν'
E.glass/Epoxy	16.8	13.9	15.0	0.2827
Graphite/Epoxy	16.3	11.5	14.6	0.2827
Isotropic	3.4	5.62	11.15	0.0

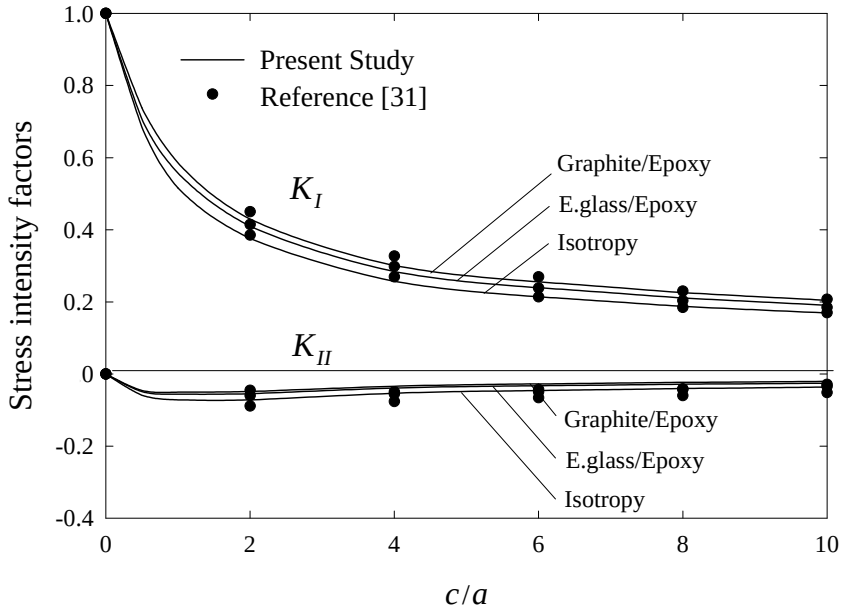

Figure 5.6 Comparison of stress intensity factors for cylindrical crack in elastic materials.

Figure 5.5 shows a comparison of crack opening displacements, $c_{44}d_r / pa$, for a pressurized crack with different crack length c/a = 0.1, 1 and 10. The solutions shown in Figure 5.5 are in very good agreement for various types of materials and different values of c/a. The comparison of solutions for the stress intensity factors $K_I / p\sqrt{\pi c}$ and $K_{II} / p\sqrt{\pi c}$ obtained from the present study and those presented by Kasano et al. [31] is shown in Figure 5.6. Very close agreement is obtained between the two sets of results. Note that electric displacement intensity factor is zero in this case.

The interface cylindrical crack in elastic fiber embedded in an infinite matrix of different elastic materials was considered by Erdogan and Ozbek [30]. The elastic constants for the fiber are E^f = 1.0×107 psi and Poisson's ratio ν =0.20, and for the matrix are E^m= 4.5×105 psi and ν =0.35. The mode I and II stress intensity factors with a/c presented by Erdogan and Ozbek [30] are compared with the present study as shown in Figure 5.7. Once again, very good agreement between the two solutions confirms the accuracy of the present scheme at the limiting case of ideal elastic composites.

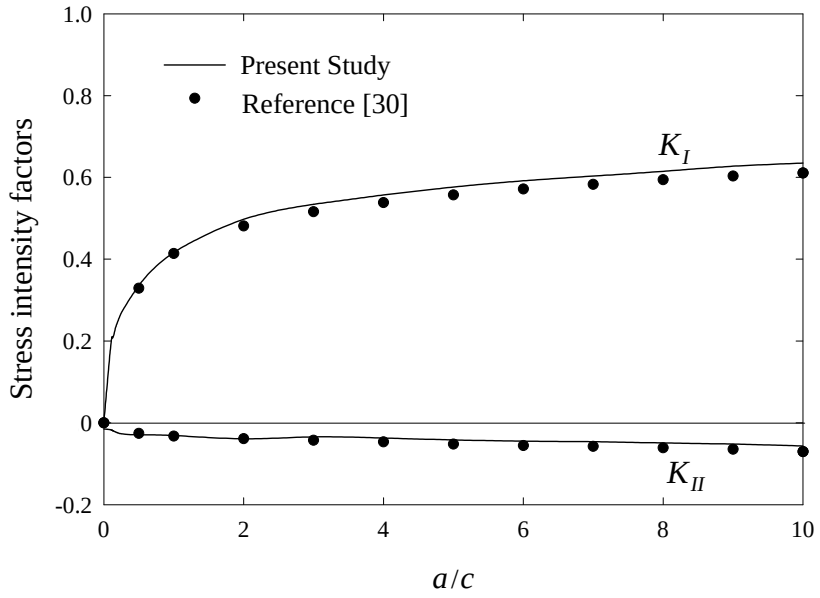

Figure 5.7 Comparison of stress intensity factors for interface crack in elastic composite.

5.2.2 Numerical Results for Single Interface Crack in Piezocomposites

The numerical results corresponding to the cylindrical crack along the interface of the piezocomposite as shown in Figure 5.1 is presented in this section. The fiber and matrix is assumed to be perfectly bonded except along the crack surfaces $(-c < z < c)$ where the constant pressure "p" is applied. The electrical boundary condition along the piezoelectric fiber interface is assumed to be electrically impermeable. Two types of piezocomposites are used in the numerical study, i.e., PZT-6B/Matrix A and PZT-6B/Matrix B. The material properties for PZT-6B, and Matrix A and Matrix B are given in Tables 1.1 and 4.1 respectively.

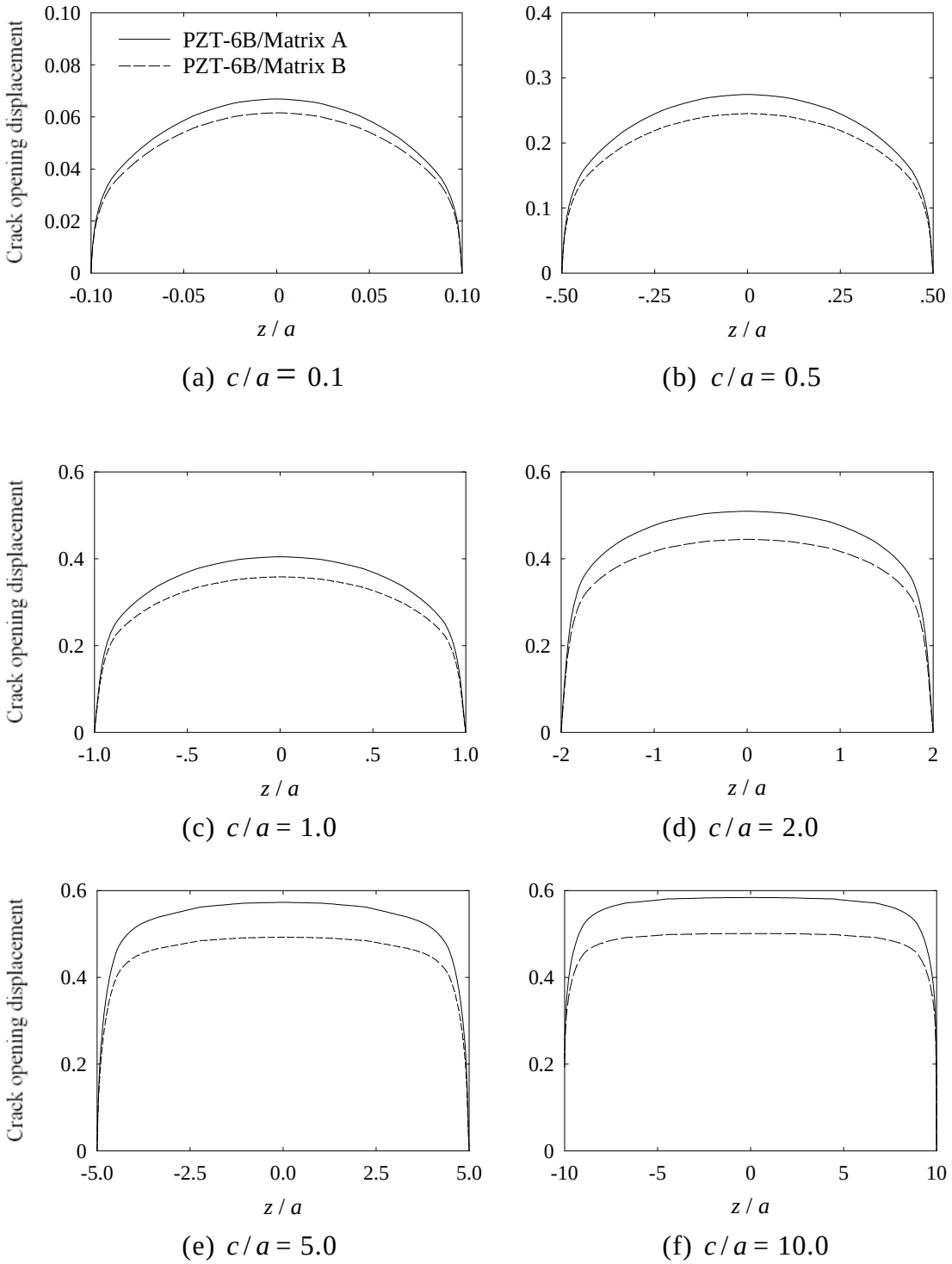

Figure 5.8 Crack opening displacements of single interface crack in piezocomposites for different c/a.

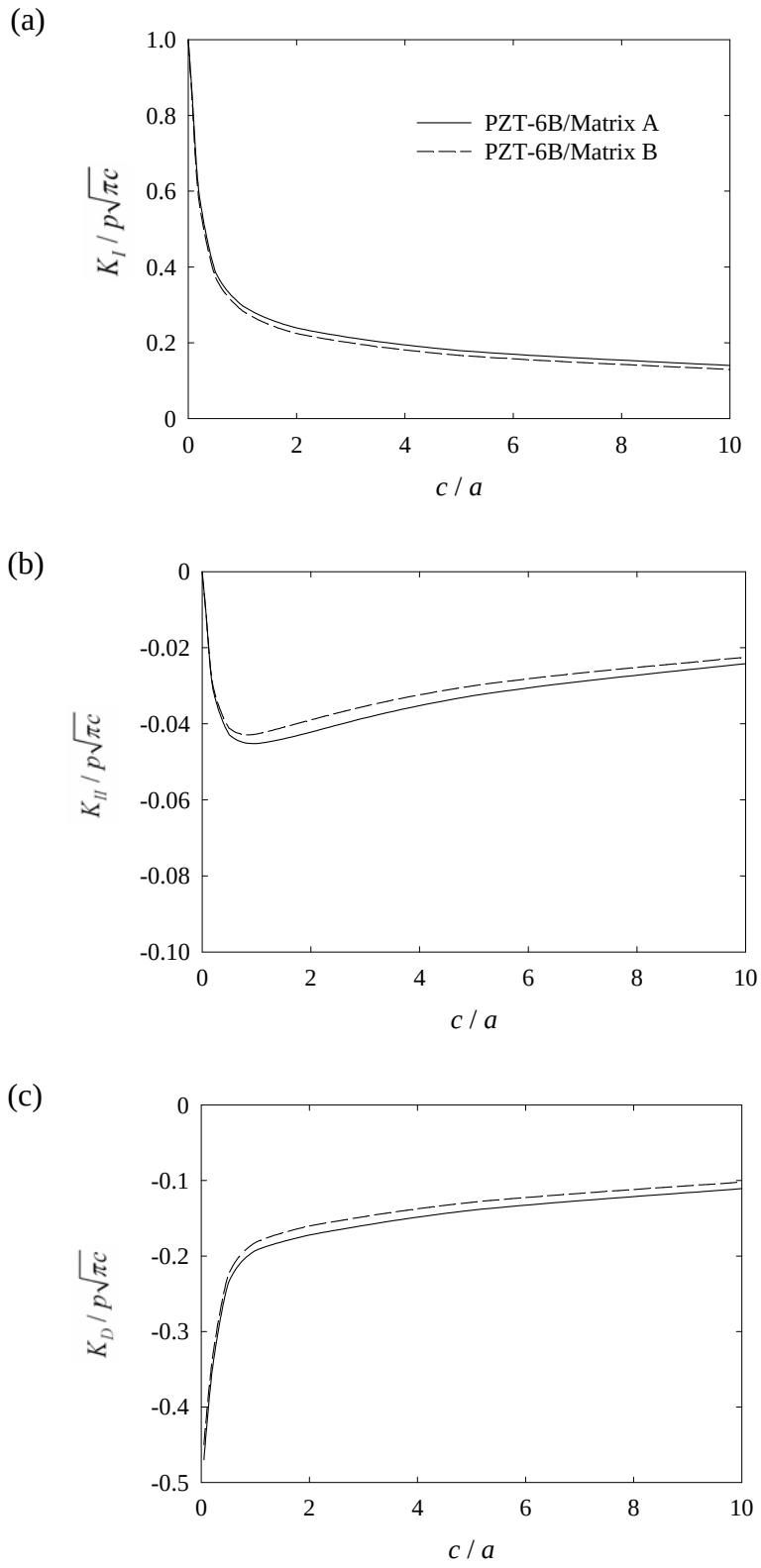

Figure 5.9 Field intensity factors of single interface crack in piezocomposites.

Figure 5.8 presents the crack opening displacement $c_{44}d_r / pa$ for different values of crack-length, i.e., c/a = 0.1, 0.5, 1, 2, 5 and 10. Numerical results presented in Figure 5.8 indicate that the displacement has the largest values at the center of the crack surfaces. The value of maximum displacements at the center increases when the crack-length increases. In addition, the profiles of the crack opening displacement in the region close to the center of the crack surface are more flat when the crack-length increases. For c/a=10, the displacement profiles are almost constant within the region -6< z/a <6. The opening displacements for piezocomposite with Matrix A are larger by 10-20% than those of Matrix B for a given crack-length. In addition, the difference in the crack opening displacements between the two composites increases when the crack-length increases.

The variations of field intensity factors $K_I / p\sqrt{\pi c}$, $K_{II} / p\sqrt{\pi c}$ and $K_D / p\sqrt{\pi c}$ with crack-length are presented in Figure 5.9. When the crack-length is sufficiently small ($c/a \to 0$), the solutions approach the plane strain solutions where Mode I stress intensity factor is independent of the material properties and K_{II} vanishes. The magnitudes of $K_I / p\sqrt{\pi c}$ and $K_D / p\sqrt{\pi c}$ decrease with increasing crack-length whereas the magnitude of $K_{II} / p\sqrt{\pi c}$ abruptly increases from zero for c/a=0 reaching the maximum value near c/a=1. It is noted that the mode II intensity factor is considerably small for a cylindrical interface crack under a constant pressure when compared to K_I and K_D. In addition, K_{III} vanishes for axisymmetric crack problem.

5.2.3 Numerical Results for Multiple Interface Cracks in Piezocomposites

The solution scheme of a single interface crack in piezocomposite presented in the foregoing section can be extended to study the interaction between multiple cracks at the interface of piezocomposite as shown in Figure 5.10.

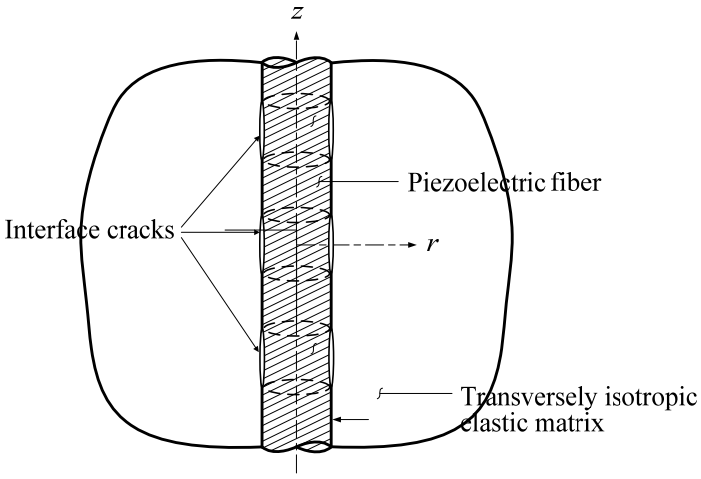

Figure 5.10 Multiple interface cracks in piezocomposites.

Consider a piezoelectric composite with two interface cracks as shown in Figure 5.11. The distance between the two crack is "*d*" and each crack has a crack length "2*c*". The electric boundary condition at the piezoelectric fiber surface is impermeable. In addition, the crack tip at the far end is denoted by "Tip A" whereas the adjacent tip is called "Tip B". The numerical results for this problem are presented in Figures 5.12-5.14.

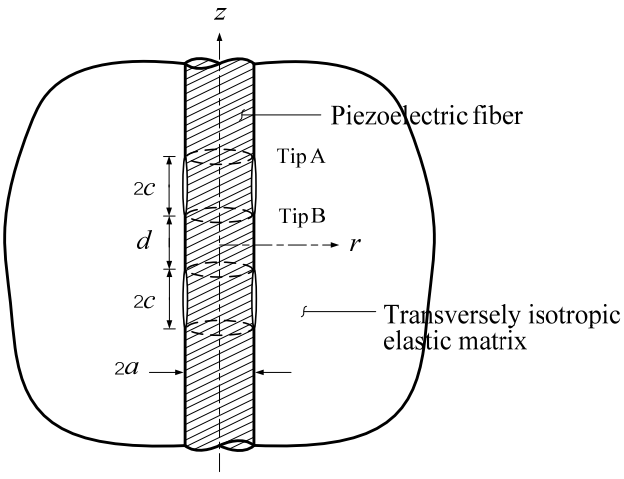

Figure 5.11 Two interface cracks problem considered in the numerical study.

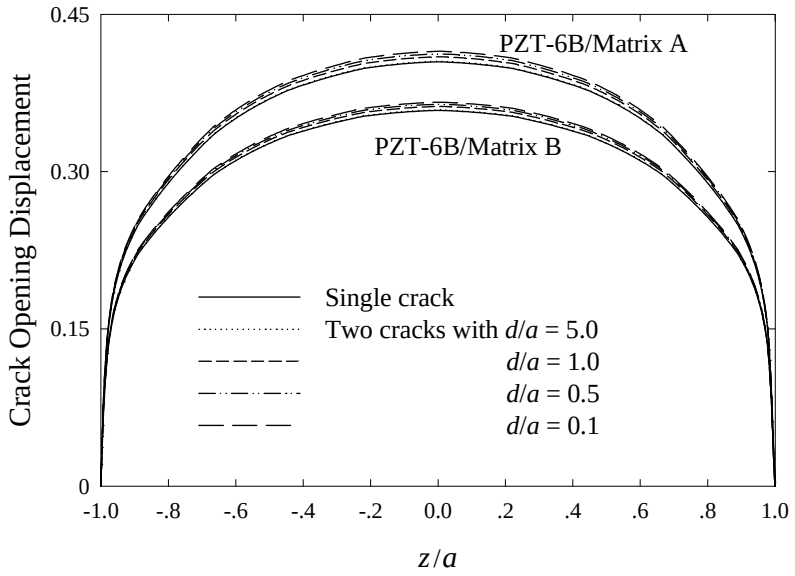

Figure 5.12 Crack opening displacements of two interface cracks in piezocomposites for different d/a.

Figure 5.12 presents the crack opening displacement of two interface cracks in PZT-6B/Matrix A and PZT-6B/Matrix B. The results are presented for different spacing between the two cracks, i.e. d/a = 0.1, 0.5, 1.0 and 5.0. It is evident from Figure 5.12 that the presence of a nearby crack results in larger crack opening displacement. In addition, the interaction between the neighboring cracks is negligible when $d/a \geq 5.0$.

Figure 5.13 presents the effect of spacing between the two interface cracks on the field intensity factors. The values of the field intensity factors corresponding to the case of a single crack are also shown in the figure as a horizontal line for comparison. It is obvious that the field intensity factors significantly increase when the interaction between multiple cracks are involved. For two cracks with c/a = 1 and spacing d/a = 0.1, all field intensity factors are more than five times higher than those of single crack of the same composite. As d/a increases, they gradually decrease approaching the single crack solutions after $d/a \geq 5.0$. In addition, the magnitudes of each intensity factor at Tip A and Tip B are not significantly different for all values of d/a.

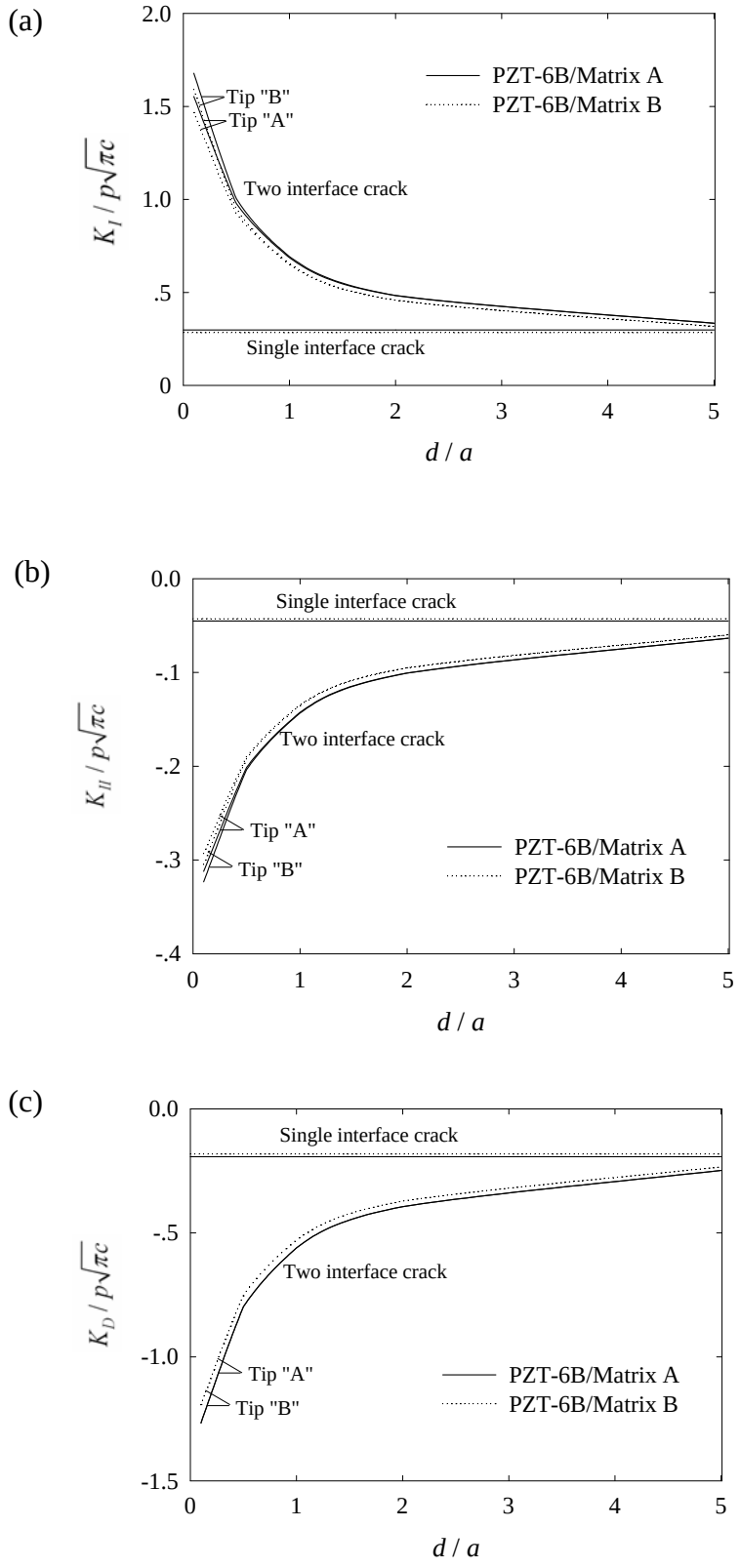

Figure 5.13 Field intensity factor for two interface cracks in piezocomposites.

CHAPTER VI

CONCLUDING REMARKS

This report presents a comprehensive theoretical study of electroelastic responses of a piezoelectric fiber-reinforced composite with the imperfect interface. The case of an infinitely long piezoelectric fiber embedded in a transversely isotropic elastic matrix is considered in the study. Both fiber and matrix are assumed to be transversely isotropic and the principal material directions are in the fiber direction. The main contributions of this research are summarized below.

1. The general solutions for coupled axisymmetric electroelastic fields of a piezoelectric material with a vertical body force and an electric body charge have been derived by using the Fourier integral transforms. The general solutions of piezoelectric materials presented in this work together with the general solutions for a transversely isotropic elastic material are useful for the study of load-transfer mechanism and interfacial fracture of piezoelectric fiber-reinforced composite.

2. The derived general solutions have been employed to solve the boundary-value problem of electromechanical load transfer and interface dislocations in piezocomposites. The fiber-matrix interface in the load transfer problem is considered to be either mechanically perfect or imperfect, and either electrically open- or short-circuited. The three–dimensional axisymmetric interfacial cracks in a 1–3 piezocomposite is also studied by adopting the displacement discontinuity method (DDM) based on the fundamental solutions of interface dislocation.

3. A computer code has been developed for analysis of axial load and electric charge transfer and interfacial fracture problem in piezocomposites. The validity and accuracy of the present solution scheme are confirmed by comparing with the existing solutions for the limiting case of ideal elastic composites reported in the literature.

4. The influence of various parameters on the axial load and electric charge transfer and interfacial fracture problem in piezocomposites has been demonstrated. The major findings from the numerical results are summarized as follows:

4.1 The coupled electro-elastic responses in piezoelectric fiber-reinforced composites are very complicated and significantly influenced by the properties of the fiber and the matrix, the electrical boundary conditions, and the interface conditions such as imperfect fiber-matrix bonding and the presence of interface cracks.

4.2 Under the application of the axial load, electric field generated in PZT-4 fiber has the highest values followed by the $BaTiO_3$ and PZT–6B fibers, which implies that PZT-4 is more suitable for sensing application. A softer matrix material results in a higher vertical electric field in the fiber as lesser load is transferred to the matrix. Nevertheless, the fiber axial force and interfacial stresses are primarily controlled by the stiffness of the matrix material and show less dependent on the piezoelectric fiber properties.

4.3 The dependence of interface stresses on the fiber and matrix material type is more pronounced in the case of electric charge loading when compared to the axial loading. Moreover, the vertical stress and electric field show a substantial dependence on the fiber type.

4.4 The presence of the imperfect interface results in lower axial load transfer to the matrix and hence lower interfacial stresses but a higher fiber vertical electrical field. In the case of electric charge transfer, interfacial stresses decrease and fiber vertical electric field increases as the interface becomes weaker.

4.5 The electric boundary condition (short- or open-circuit) of the fiber shows significant influence on the fiber electric field and interfacial stresses particularly in the electric charge loading case.

4.6 The numerical examples for interface cylindrical crack in piezocomposite show that a crack opening displacement, and stress and electric displacement factors significantly depend on the composite properties and the ratio of crack-length to fiber radius (c/a).

4.7 The opening displacement is maximal at the center of the crack surfaces and the value of maximum displacement increases when the crack-length increases. For the limiting case of a vanishingly small crack-length ($c/a \to 0$), the mode I stress intensity factor is independent of the composite material while the mode II intensity factor vanishes. The electric displacement intensity factor $K_D / p\sqrt{\pi c}$ is maximum when c/a=0 and decreases as c/a increases.

4.8 The numerical results from the case of multiple interface cracks reveal that the influence from a nearby crack is more obvious in the case of field intensity factor when compared to the case of opening displacement. The interaction between neighboring cracks becomes negligible when the distance between the adjacent crack tip is more than five times of the fiber radius.

The results presented in this research project provide a fundamental understanding of coupled electro-mechanical responses in the composite of piezoelectric materials. Based on the solution procedure developed in this project, the composites of piezomagnetic materials can also be studied. In addition, the approach presented in this report can be extended to investigate more complicated problems such as piezocomposite with different fiber cross sections; the investigation of the fiber-to-fiber interaction; and the determination of the effective electro-mechanical properties of piezoelectric fiber-reinforced composite by employing micromechanics approach.

REFERENCES

[1] Crawley, E.F., Intelligent structures for aerospace: A technology overview and assessment. AIAA J., 1994, 32, 1689-1699.

[2] Rao, S.S. and Sunar, M., Piezoelectricity and its use in disturbance sensing and control of flexible structures: A survey. Appl. Mech. Rev., 1994, 47, 113-123.

[3] Mindlin, R.D., Equations of high frequency vibrations of thermopiezoelectric crystal plates. Int. J. Solids Structures, 1974, 10, 625 -637.

[4] Chen, PJ., Three-dimensional dynamic electromechanical constitutive relations for ferroelectric materials. Int. J. Solids Structures, 1980, 16, 1059-1067.

[5] Deeg, W.F. The analysis of dislocation, crack and inclusion problems in piezoelectric solids, Ph.D Thesis, Stanford University, CA, USA, 1980.

[6] Parton, V.Z. and Kudryavtsev, B.A., Electromagnetoelasticity, Gordon and Breach Science Publishers, New York, 1988.

[7] Sosa, H., Plane problems in piezoelectric media with defects. Int. J. Solids Structures, 1991, 28, 491-505.

[8] Rajapakse, R.K.N.D., Plane strain/stress solutions for piezoelectric solids. Composites, 1997, 28B, 385-396.

[9] Xu, X.L. and Rajapakse, R.K.N.D., A theoretical study of branched cracks in piezoelectrics. Acta mater., 2000, 48, 1865-1882

[10] Xu, X.L. and Rajapakse, R.K.N.D., On a plane crack in piezoelectric solids. Int. J. Solids Structures, 2001, 38, 7643-7658.

[11] Rajapakse, R.K.N.D. and Zhou, Y., Stress analysis of piezoceramic cylinders. Smart Mat. Structures, 1997, 6(2), 169–177.

[12] Rajapakse, R.K.N.D., Chen , Y. and Senjuntichai, T., Electroelastic field of a piezoelectric annular finite cylinder. Int. J. Solids Structures, 2005, 42, 3487–3508.

[13] Senjuntichai, T., Kaewjuea, W. and Rajapakse, R.K.N.D., Piezoelectric cylinder under voltage and axial loading. Int. J. Applied Electromagnetics Mechanics, 2008, 27, 93-116.

[14] Hagood, N.W. and Bent, A.A., Development of piezoelectric fiber composite for structural actuation. Proc. 34th AIAA/ASME/ASCE/AHS Structures, Structural Dynamics and Materials Conference, AIAA paper no. 93-1717, La Jolla, CA, 1993.

[15] Newnham, R.E., Bowen, L.J., Klicher, K.A. and Cross L.E., Composite piezoelectric transducers. Materials Eng., 1980, 2, 93-106.

[16] Muki, R. and Sterberg, E., On the diffusion of an axial load from an infinite cylindrical bar embedded in an elastic medium. Int. J. Solids Structures, 1969, 5, 587-605.

[17] Pak, R.Y.S. and Gobert, A.T., Axisymmetric problems of a partially embedded rod with radial deformation. Int. J. Solids Structures, 1993, 29, 1745-1759.

[18] Slaughter, W.S. and Sanders, Jr., J.L., A model for the load-transfer from an embedded fiber to an elastic matrix. Int. J. Solids Structures, 1991, 28, 1041-1052.

[19] Niumpradit, B. and Karasudhi, P., Load transfer from an elastic pile to a saturated porous elastic soil. Int. J. Numer. and Anal. Meth. Geomech., 1981, 5, 115–138.

[20] Selvadurai, A.P.S. and Rajapakse, R.K.N.D., Axial stiffness of anchoring rods embedded in elastic media. Can. J. Civ. Eng., 1990, 17(3), 321–328.

[21] Senjuntichai, T., Sornpakdee, N., Teerawong, J., Rajapakse, R.K.N.D., Time dependent response of an axially loaded elastic bar in a multi-layered poroelastic medium. J. Engng. Mech.-ASCE, 2007, 133, 578-587.

[22] Mal, A.K. and Bose, S.K., Dynamic elastic moduli of a suspension of imperfectly bonded spheres. Proc. Cambridge Phil. Soc., 1975, 76, 587–600.

[23] Nairn, J.A. and Liu, Y.C., Stress transfer into a fragmented anisotropic fiber through an imperfect interface. Int. J. Solids Structures, 1996, 34, 1255-1281.

[24] Lenci, S. and Menditto, G., Weak interface in long fiber composites. Int J Solids Structures, 2000, 37, 4239–4260.

[25] Aveston, J., Cooper, G.A. and Kelly, A., Single and multiple fracture, in The Properties of Fiber Composites Conference Proceedings National Physical Laboratory, Teddington, U.K. IPC Science and Technology Press, Surrey, 1971, 15–26.

[26] Marshall., D.B., Cox, B.N. and Evans, A.G., The mechanics of matrix cracking in brittle–matrix fiber composites. Acta Metall., 1985, 33, 2013–2021.

[27] McCartney, L.N., Mechanics of matrix cracking in brittle-matrix fiber-reinforced composites. J. Roy. Soc. Lond., 1987, A409, 329–350.

[28] Wijeyewickrema, A.C., Keer, L.M., Hirashima, K. and Mura, T., The annular crack surrounding an elastic fiber in a tension field. Int. J. Solids Structures, 1991, 27, 315–328.

[29] Wijeyewickrema, A.C. and Keer, L.M., Matrix fracture in brittle matrix fiber reinforced composites. Int. J. Solids Structures, 1991, 28, 43–65.

[30] Erdogan, F. and Ozbek, T., Stresses in fibre-reinforced composites with imperfect bonding. J. Appl. Mech., 1969, 36, 865–869.

[31] Kasano, H., Matsumoto, H. and Nakahara, I., A torsion–free axisymmetric problem of a cylindrical crack in a transversely isotropic body. Bulletin of Japan Soc. Mech. Engrs, 1984, 27(229), 1323–1332.

[32] Yang, S. and Yuan, F.G., Interfacial circular crack in cylindrically anisotropic composites under antiplane shear. Int. J. Solids Structures, 1995, 32(24), 3603–3622.

[33] Farris, T.N., Kokini, K. and Demir, I., The cylindrical crack. J. Appl. Mech., 1989, 56, 981-983.

[34] Demir, I, Hirth, J.P. and Zbib, H.M., The extended stress field around a cylindrical crack using the theory of dislocation pile-ups. Int. J. Engng Sci., 1992, 31, 829-845.

[35] H. M. Zbib, J. P. Hirth, I. Demir, The stress intensity factor of cylindrical cracks. Int. J. Engng Sci. Vol. 33 No. 2 (1995) 247-253.

[36] Zhang, T.Y., Zhao, M.H. and Tong, P., Fracture of piezoelectric ceramics. Adv. Appl. Mech., 2002, 38, 148–289.

[37] Sosa, H., On the fracture mechanics of piezoelectric solids. Int. J. Solids Structures, 1992, 29, 2613–2622.

[38] Suo, Z., Kuo, C.M., Barnett, D.M. and Wilis, J.R., Fracture mechanics for piezoelectric ceramics. J. Mechs. Phys. Solids, 1992, 40(4), 739–765.

[39] Tian, W.Y. and Rajapakse, R.K.N.D., Fracture parameters of a penny shaped crack at the interface of a piezoelectric bi-material system. Int. J. Fract., 2006,141, 37–48.

[40] Xu, X.L. and Rajapakse, R.K.N.D., On singularities in composite piezoelectric wedges and junctions. Int. J. Solids Structures, 2000, 37, 3253–3275.

[41] Cruise, T.A., Boundary element analysis in computational fracture mechanics. Kluwer academic publishers, Boston, 1988.

[42] Pan, E., A BEM analysis of fracture mechanics in 2D anisotropic piezoelectric solids. Engrg. Anal. Bound. Elem., 1999, 23, 67–76.

[43] Zhao, M.H., Fang, P.Z. and Shen, Y.P., Boundary integral–differential equations and boundary element method for interfacial cracks in three-dimensional piezoelectric media. Eng. Anal. Boundary Elem., 2004, 28, 753–762.

[44] Crouch, S.L. and Starfield, A.M., Boundary Element Methods in Solid Mechanics. George Allen and Unwin, London, 1983.

[45] Bilby, B. and Eshelby, J.D., Dislocations and the theory of fracture, in Liebowitz, H. (eds.), Fracture, pp 99–182, Academic press, New York, 1968.

[46] Pak, Y.E., Linear electroelastic fracture mechanics of piezoelectric materials. Int. J. Fracture, 1992, 54, 79–100.

[47] Sladek, V. and Sladek, J., Three-dimensional crack analysis for anisotropic body. Appl. Math. Model., 1982, 6, 374–380.

[48] Ou, Z.C. and Wu, X., On the crack-tip stress singularity of interfacial cracks in transversely isotropic piezoelectric bimaterials. Int. J. Solids Structures, 2003, 40, 7499–7511.

[49] Ou, Z.C. and Chen, Y.H., Interface crack problem in elastic dielectric/piezoelectric bimaterials. Int. J. Fracture, 2004, 130, 427–454.

[50] Wang, Z. and Zheng, B. , The general solution of three-dimensional problems in piezoelectric media. Int. J. Solids Structures, 1995, 32, 105–115.

[51] Sneddon, I., The use of integral transforms. New York, McGraw-Hill, 1970.

[52] Watson, G.N., A treatise on the theory of bessel functions. Cambridge University Press, 1962.

[53] Piessens, R., deDoncker, E., Uberhuber, C. and Kahaner, D., QUADPACK: a subroutine package for automatic integration. Berlin: Springer, 1983.

[54] Stroh, A.N., Steady state problems in anisotropic elasticity. Journal of Mathematics and Physics, 1962, 41, 77–103.

[55] Lekhnitskii, S.G., Theory of Elasticity of an Anisotropic Elastic Body. Holden-Day, New York, 1963.

[56] Herrmann, K.P., Loboda, V.V. and Govorukha, V.B., On contact zone models for an electrically impermeable interface crack in a piezoelectric biomaterial. Int. J. Fracture, 2001, 111, 203–227.

[57] Herrmann, K.P. and Loboda, V.V., Fracture mechanical assessment of interface cracks with contact zones in piezoelectric bimaterials under thermoelectromechanical loadings I. Electrically permeable interface cracks. Int. J. Solids Structures, 2003, 40, 4191–4217.

[58] Ting, T.C.T., Explicit solution and invariance of the singularities at an interface crack in anisotropic composites. Int. J. Solids Structures, 1986, 9, 965–983.

[59] Abramowitz, M. and Stegun, I.A., Handbook of Mathematical Functions. Dover Publications, Inc., New York, 1970.

OUTPUT

1. International Journal

- Sapsathiarn Y, Senjuntichai T, Rajapakse RKND. Electro-mechanical load transfer from a fiber in a 1-3 piezocomposite with an imperfect interface. Composites Part B: Engineering 2008, 39: 1114-1124.

2 International Conference Proceeding

- Sapsathiarn Y, Senjuntichai T, Rajapakse RKND. Axial load transfer from a piezoelectric cylindrical fiber into a transversely isotropic elastic matrix. The International Conference on Smart Materials and Nanotechnology (SMN 2007), Harbin, China, July, 2007.
- Sapsathiarn Y, Senjuntichai T, Rajapakse RKND. Modeling of Interfacial Cracks in 1-3 Piezocomposites. The 1st Asean Civil Engineering Conference (ACEC 2009), Pattaya, Thailand, March, 2009.

APPENDIX

1. Sapsathiarn Y, Senjuntichai T, Rajapakse RKND. Electro-mechanical load transfer from a fiber in a 1-3 piezocomposite with an imperfect interface. Composites Part B: Engineering 2008, 39: 1114-1124.
2. Sapsathiarn Y, Senjuntichai T, Rajapakse RKND. Axial load transfer from a piezoelectric cylindrical fiber into a transversely isotropic elastic matrix. The International Conference on Smart Materials and Nanotechnology (SMN 2007), Harbin, China, July, 2007.
3. Sapsathiarn Y, Senjuntichai T, Rajapakse RKND. Modeling of Interfacial Cracks in 1-3 Piezocomposites. The 1st Asean Civil Engineering Conference (ACEC 2009), Pattaya, Thailand, March, 2009.